Amyloid β peptide: from monomer solubility to fibril structure

Lattanzi, Veronica

2021

Amyloid β peptide:

from monomer solubility to fibril structure

VERONICA LATTANZI | BIOCHEMISTRY AND STRUCTURAL BIOLOGY | LUND UNIVERSITY

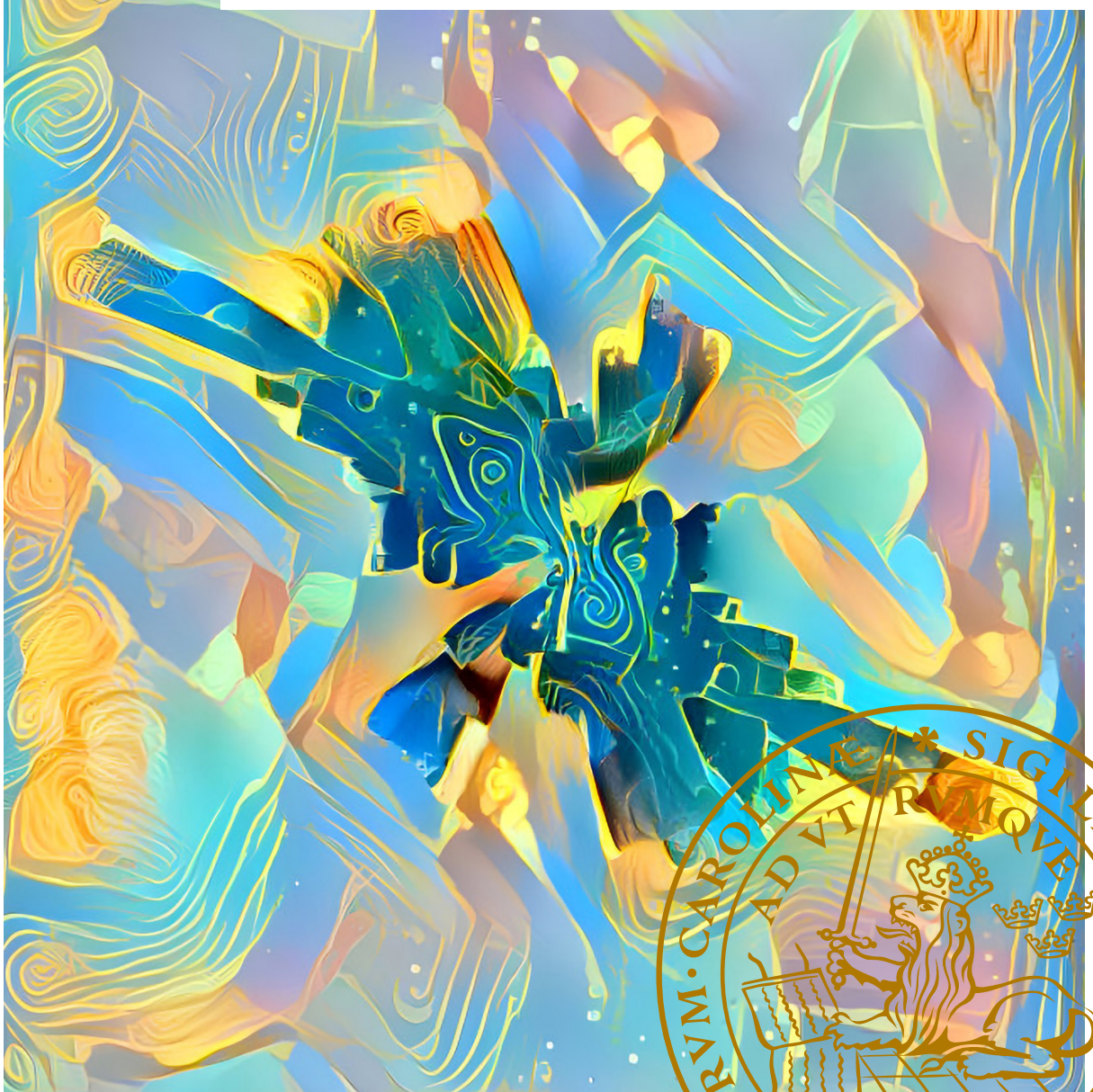

Alzheimer's disease is the most common human neuro-degenerative disorder and is characterized by the formation of cerebral plaques. It is widely believed that the production and deposition of Amyloid-β peptides in the human brain might be one of the causative agents of the disease.

This thesis presents the development of a bottom-up protocol for the in vitro detection of the solubility of Amyloid-β40 peptide in pure buffer conditions, i.e. the concentration in solution at equilibrium.

The second part of the thesis focuses on the investigation of the structures formed at the end state of fibril formation. A model calculation, based on neutron and X-ray small angle scattering data, is proposed for the determination of Amyloid-β fibril shape, cross-section dimensions and most importantly, the number of filaments.

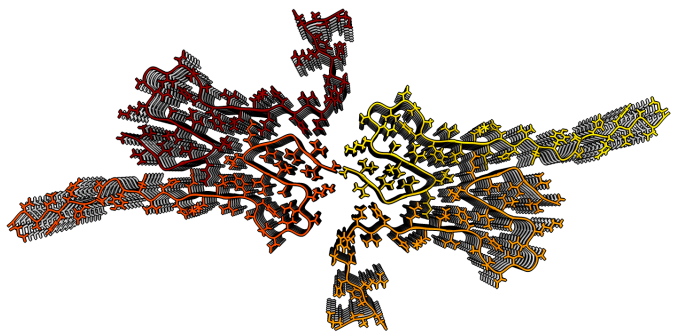

Printed by Media-Tryck, Lund 2021 NORDIC SWAN ECOLABEL 3041 0903

LUND UNIVERSITY

ISBN: 978-91-7422-848-9

Biochemistry and Structural Biology
Faculty of Science
Lund University

Amyloid β peptide: from monomer solubility to fibril structure

Amyloid β peptide: from monomer solubility to fibril structure

by Veronica Lattanzi

LUND
UNIVERSITY

Thesis for the degree of Doctor in Philosophy

by due permission of the Faculty of Science, Lund University, Sweden.
To be defended on Friday, the 17th of December 2021 at 13:00 in Lecture hall C at the Department of Chemistry, Lund University.

Faculty opponent

Prof. Annette Eva Langkilde
University of Copenhagen

Organization
LUND UNIVERSITY
Department of Chemistry
Box 124
SE–221 00 LUND
Sweden

Document name
DOCTORAL DISSERTATION

Date of disputation
2021-12-17

Sponsoring organization

Author(s)
Veronica Lattanzi

Title and subtitle
Amyloid β peptide: from monomer solubility to fibril structure:

Abstract

Alzheimer´s disease (AD) is the most common human neuro-degenerative disease characterized by the formation of cerebral plaques. Several are the amyloid-beta (Aβ) variants found in the brain of healthy individuals. Among them, the Aβ40 variant is predominantly found in the cerebrospinal fluid while the Aβ42 variant appears as fibrillar aggregates in the brain of AD patients. In vitro studies confirm that Aβ42 is more aggregation prone than Aβ40; however, it is difficult to determine the solubility in a complex environment such as the human brain. The propensity of Aβ fibrils to catalyze the formation of new aggregates via the interaction of soluble monomers with the fibril surface, drives the attention towards Aβ fibril structures; however, a detailed model for these structures is lacking.

This thesis presents the development of a bottom-up protocol for the in vitro detection of the solubility of Aβ40 peptide in pure buffer conditions, i.e. the concentration in solution at equilibrium. It is shown that by working with peptides that are recombinantly expressed in E. coli cells and purified to high homogeneity, the aggregation propensity of Aβ40 peptide can be measured in vitro via systematic and reproducible solubility studies.

The second part of the thesis focuses on the investigation of the structures formed at the end state of fibril formation. A model calculation is here proposed for the determination of Aβ fibril shape, cross-section dimensions and most importantly, the number of filaments based on small angle scattering data. The relation between Aβ40 and 42 variants' solubility concentrations and the high resolution structures of Aβ fibrils can help design experiments to elucidate the factors that cause AD and provide a basis for the development of more effective treatments.

Key words
Alzheimer´s disease, Aβ solubility, small angle scattering, number of filaments, fibril structure, Aβ40, Aβ42, Aβ42 S26Q

Classification system and/or index terms (if any)

Supplementary bibliographical information

Language
English

ISSN and key title

ISBN
978-91-7422-848-9 (print)
978-91-7422-849-6 (pdf)

Recipient's notes

Number of pages
173

Price

Security classification

Signature  Date 2021-11-08

Amyloid β peptide: from monomer solubility to fibril structure

by Veronica Lattanzi

LUND
UNIVERSITY

This doctoral thesis is constructed as a summary of research papers and consists of three parts. An introductory text puts the research work into context and summarizes the main conclusions of the papers. Then, the research publications themselves are reproduced. Two research papers are published and two are manuscripts.

Figure 1 The author.

Faculty of Science, Department of Chemistry, Division of Biochemistry and structural biology

ISBN: 978-91-7422-848-9 (print)
ISBN: 978-91-7422-849-6 (pdf)

Printed in Sweden by Media-Tryck, Lund University, Lund 2021

Media-Tryck is a Nordic Swan Ecolabel certified provider of printed material. Read more about our environmental work at www.mediatryck.lu.se
MADE IN SWEDEN

Table of Contents

Acknowledgments

Tjatåsvane, home/office, 2021-07-17
(five months from the PhD defense)

I would like to start by thanking my Supervisors: Sara, Ulf and Emma. It was so beneficial to work in a team of people that I could relate with. Thanks for the opportunity you gave me.
Sara, it was the best PhD one could have ever asked for. Thanks for guiding me with humor, for being an example for me in many ways, for the stolen smiles in the corridor in between experiments, for the fun when playing games, for the trust I was given to explore different projects in an independent way. Tusen tack!
Ulf. Thanks for the mentorship. For supporting an inclusive working environment at Physical Chemistry and for always being so supportive with everyone. Thanks for the scientific discussions: at the white board, during walks, group meetings, while eating good food, or on zoom. Thanks for pushing my limits. Last but not least, thanks for the basketball matches (I can not believe you are still so good). Grazie mille!
Emma thank you for the co-supervision and for always being a valid guide and support for your students. I enjoyed the times I took part your group meetings to learn more about lipids, skin tissue, alpha synuclein..the soft matter of the world. I am grateful I got to work together with you and your group. Thanks!
To all the people I have worked closely with and to the projects collaborators. **Birigitta**, I felt so privileged to have you there at the beginning of my PhD. You taught me well. **Katija**, if I think about MS, I smile. I enjoyed our moments of knowledge infusion. **Ingemar**, thanks for our scientific discussions and your great humor. **Martin**, thanks for always being helpful with every young scientist in the group. **Karin Å.**, thanks for your energy at work. It is always nice to see you in the lab and elsewhere. **Marija**, I will never forget the beamtimes, working together while listening ACDC during the night shifts. Thanks for the moments we shared together in Sweden and elsewhere. **Kalyani**, thanks for being so kind with everyone and for the collaboration with S26Q mutant. **Salima B.**, we only met via zoom meetings. Thanks for the great collaboration and for the knowledge exchange with a sense of Italian-American humor.
Rebecca, my first office mate. Thanks for the friendship and kindness. **Mattias**, thanks for the laughter, the friendship and for teaching with me

before and during the pandemic. **Tinna**, thanks for the funny times in the lab and elsewhere. Thanks to Mitra´s smiles, she made my days during the pandemic. **Dev**, thanks for being kind and available with everyone when needed. **Tanja**, it is so nice to have you back. **Egle**, thanks for the laughter, you are such a nice person. **Christin**, it is always so nice to talk to you about science or anything else. **Lei**, my second office mate. Thanks for carrying together the battle that Spaniards and Italians do not have to necessary follow some stereotypes. **Eimantas**, you are a talented and kind person. **Max and Emil**, it has been such a great fun talking endlessly about science with you. **Thom**, thanks for being there for us and..for the plate readers. **Janina S.** thanks for sharing your curiosity for the enzymes with me and for making my dream come true (to drive the Volkswagen camper van!)

To my friends and colleagues at the CMPS and Physical Chemistry, to the past and new members. It has been an incredible pleasure to be surrounded by you all. Thanks for the stimulating scientific discussions, for having contributed to an open minded and familiar working environment. You are all talented and equally dear to me.

Magnus and Maryam, thanks to keep up the good work at the CMPS. **Tommy, Cecilia, Susanna, Sofi, Hurban and Christin**: thanks for being always kind to everyone. **Salam**, thanks for helping me out with the Russian visa. **Erik**, thanks for sharing with us the precious Ven Spirit of Hven. Thanks to **Mads, Camille, CJ, Sven, Helin, Balder, Mathias, Filip, Olof. Bhakat and Samuel** for the movie nights, beer-jazz clubs, Christmas parties, cooking nights, BBQs, for my first ginger bread house (Max I am so proud of our floating Nobel-UP).

Axel, Erika, Victoria and Brett. It was such a great fun to work together and to see you in the office during my missions at the other side of the corridor. Thanks for our outdoor activities and for the lovely picnics. **Ricardo G.**, I kept my promise. I hope I will visit you and your lovely family in Portugal soon. **Luigi G.**, thanks for being the kind of scientist I could endlessly talk to. **Marta G.**, to the question, where we are and where we are going, I answer: we are cool. **Jun, Kasia, Alexandra, Simon, Marco F. and Jing**, thanks for the interesting scientific discussions during the group meetings. Thanks to **Maria L., Maria S. and Christopher W.** to keep up the good work at Physical Chemistry. **Peter H.** for taking care of the Ganesha so well. **Cinzia G.** thanks for the scientific discussions, for the friendship and for introducing me to sailing. **Jannette C.** thanks for the friendship, for sharing interesting articles, for the movie nights and for your delicious sallad nicoise.

Thanks to **Bea, Silvia, Thomas, Yizhaq and Luis**, for the time we spent together at the Ulm conference and for the scientific discussions. Thanks to **Luciano G.** for introducing me to the incredible research environment in Lund. Thanks to **the LINXS board** for supporting my creative ideas and for the freedom I was given with the webinars series. Thanks to **the NDR members** for the work done together while representing the PhD students at the Kemicentrum. **Smita and Malin** it was fun to work with you. Thanks to **the NIST PhDs** I shared the office with, for the scientific discussions and the nice evenings in Washington.
I also want to thanks those who during the past four years included me in their own unique world and accepted mine. Thanks to those I found by my side (in person or remotely), to those who made my day with a kind gesture or word, you know who you are. Thanks to **Cecilia, Ermioni, Stella, Jasmin, Lorenzo, Tummins, Aljoša, Giovanni, Maria, Rita, Valeria, Roberta, Jessica, Alfred, Giuseppe, Monica, Stefano, Eva, Emil, Anton, Teodor, Helena, Nicola and Beatrice**. I am tankful for the laughter, for the escapes into the nature, for the home made food, for the moments of creativity and for including me in your family traditions. Thanks to my Svanegatan brothers **Louis and Jeremy**. Dancing in the kitchen is the way. Thanks to **Giulio and Kush** to be like a family to me. Per il ciambellone fatto in casa a colazione la domenica mattina and our questionable music taste. Thanks to **Marco and Alberto** for the brotherhood that we have shared since we were 18 years old. **Martina**, thanks for being my friend since we were 6 years old. It was beautiful to grow up with you in a simple and authentic way, close to the Mediterranean Sea, Rome and the beautiful Abruzzo mountains. **To my relatives all over the world**. Thank you for finding the time to meet and share funny moments with me. A special thanks to my nephews for your smiles.
Grazie a **mia Madre e a mio Padre**, for teaching me that there are no shortcuts to any place worth going. Vi voglio bene.
Nonna e Nonno thanks for the unconditional love you gave me.
Andrea, I am so grateful to be your sister. Thanks for the laughter, for our adventures and for being my best friend. Onwards, Aoshima!

With Love,
Vero
(sitting in the sunshine)

Popular scientific summary

Personally, I don't particularly enjoy sweet tea but for the sake of this protein metaphor let's say we like it. We like it so much that after the first teaspoon of sugar in our tea, we add another ten! It is winter, so everyone likes to drink pretty hot tea. The temperature is hot enough that all the sugar dissolves, making our tea a solution with a high sugar content. Now after a few sips of this sugar bomb, we put it down and decide not to finish it (understandable!). As the temperature drops to room temperature, there will now be more dissolved sugar than the water can actually hold - we call this a supersaturated solution. A supersaturated solution is not stable, meaning that the sugar in excess in our cold tea will separate from the solution and fall back into solid sugar. We call this separation a phase transition. The phase transition continues until the solution is no longer supersaturated, meaning that we have reached an equilibrium between dissolved and solid sugar.

While a supersaturated sugar tea might not taste well, scientific studies on human diseases suggest that supersaturated protein solutions in our brains can be very bad as well. For such protein solutions, an equivalent phase transition to the solidification of the sugar in our tea can be the formation of amyloid fibrils in the human body. These can cause terrible diseases such as diabetes type 2, Parkinson's disease, and the most common type of dementia - Alzheimer's disease.

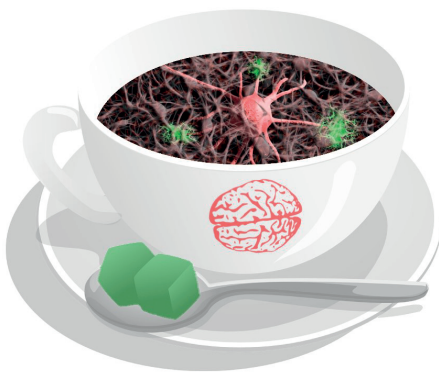

A cup of sweet tea, or a supersaturated protein solution with risk of aggregating into amyloid plaques in the brain?

To be fair, it's not necessarily bad to have proteins in our body. Proteins are

after all the main component of our organs, bones, muscles, skin and nails. They are versatile building blocks of life and consist of endless combinations of only 20 different amino acids. However, protein solutions can become a problem as they go through the phase transition to form amyloid fibrils. These fibrils have been found as plaque in the brains of Alzheimer's patients and are connected to brain tissue loss.

When it comes our sugar-in-tea example we have a good understanding of how properties like temperature and sugar concentration interplay in the phase transition, but for amyloid fibrils we still need to learn more. The development of effective treatments against Alzheimer's disease requires a good understanding of both how amyloid fibrils form and what their structures look like. In this thesis I developed a method to detect the concentration of one kind of amyloids in solutions and measured at which total concentration the phase transition to fibrils begins and reach the equilibrium state. With the fibrils, I then took the next step towards understanding their structure using an in-house X-ray source and a neutron source in Switzerland. In the future, it will be possible to do these kinds of studies at MAX IV and the European Spallation Source (ESS) in Lund. Hopefully soon, incurable diseases such as Alzheimer's disease and other protein aggregated disorders will be left behind as part of history. But even then please, one teaspoon of sugar is plenty.

List of Publications

This thesis is based on the following publications, referred to by their Roman numerals:

I **Solubility of Aβ40 peptide**

V. Lattanzi, K. Bernfur, E. Sparr, U. Olsson, S. Linse
JCIS Open, 100024 DOI: 10.1016/j.jciso.2021.100024 **2021**

II **Amyloid β 42 fibril structure based on small angle scattering**

V. Lattanzi, A. Ingemar, U. Gasser, M. Dubackic, U. Olsson, S. Linse
Proc. Natl. Acad. Sci. **2021**, in press

III **Structural characterization of Aβ1-40 amyloid fibrils using magic angle spinning nuclear magnetic resonance**

S. Bahri, R.P.G. Silvers, B. Michael, **V. Lattanzi**, I. André, U. Olsson, R.G. Griffin, S. Linse
To be submitted

IV **On the role of phosphorylation of serine residues in aggregation mechanism of amyloid β-peptide**

K. Sanagavarapu, G. Meisl,**V. Lattanzi**, K. Bernfur, B. Frohm, U. Olsson, T. PJ Knowles, A. Malmendal, S. Linse
To be submitted

Publications not included in this thesis:

On the cluster formation of alpha-synuclein fibrils

M. Dubackic*, I. Idini*,**V. Lattanzi**, Y. Liu, A. Martel, A. Terry, M. Heartlein, J. Devos, A. Jackson, E. Sparr, S. Linse, U. Olsson
Frontiers, **2021**

Surface-catalyzed secondary nucleation dominates the generation of toxic IAPP aggregates

D.C. Rodriguez Camargo, S. Chia, J. Menziez, B. Mannini, G. Meisl, M. Lundqvist, K. Bernfur,**V. Lattanzi**, J. Habchi, S. Cohen, T. PJ Knowles, M. Vendruscolo, S. Linse
Frontiers, **2021**

Sphere - Tubule Superstructures through Supramolecular and Supracolloidal Assembly Pathways

J.Cautela, **V. Lattanzi**, L. K. Månsson, L. Galantini, J. J. Crassous
Small, **2018**

Monomeric and fibrillar α-synuclein exert opposite effects on the catalytic cycle that promotes the proliferation of Aβ42 aggregates

S. Chia, P. Flagmeier, J. Habchi,**V. Lattanzi**, S. Linse, C.M. Dobson, T. Knowles,M. Vendruscolo
PNAS, **2017**

My contributions to the papers

Paper I

I took part in the design of the study. I performed the size exclusion purification of Aβ40. I prepared all the samples, designed and performed all the experiments. I analyzed the data and contributed to the data interpretation. I wrote the first draft of the manuscript and revised with inputs from the co-authors.

Paper II

I took part in the design of the study. I performed the size exclusion purification of Aβ42. I prepared all the samples, designed and performed the X-ray experiments using a Saxslab Ganesha pinhole instrument. I prepared the samples and took part at the small angle neutron experiment at SINQ, Paul Scherrer Institute. I analyzed and contributed to data interpretation. I wrote the first draft of the manuscript and edited it with inputs from the co-authors.

Paper III

I took part in the design of the small angle X-ray study. I performed the size exclusion purification of Aβ40. I prepared all the samples and performed the experiments using a Saxslab Ganesha pinhole instrument. I analyzed the data and contributed to the data interpretation. I wrote the corresponding part on the manuscript and revised it with inputs from the co-authors.

Paper IV

I took part in the design of the small angle X-ray study. I performed the size exclusion purification of S26Q. I prepared all the samples and performed the experiments using a Saxslab Ganesha pinhole instrument. I analyzed the data and contributed to the data interpretation. I wrote the corresponding part of the manuscript and revised it with inputs from the co-authors.

Abbreviations

AD Alzheimer´s Disease

APP Amyloid Precursor Protein

Aβ Amyloid-β peptide

cryo-EM Cryogenic Electron Microscopy

CSF Cerebrospinal Fluid

D_2O deuterium oxide/heavy water

FDA Food and Drug Administration

IDP Intrinsically Disordered Peptide

MALDI Matrix assisted laser desorption ionization

MDS Microfluidic diffusional sizing

SANS Small Angle Neutron Scattering

SAS Small Angle Scattering

SAXS Small Angle X-ray Scattering

SEC Size Exclusion Chromatography

SLD Scattering Length Density

ss-NMR solid state Nuclear Magnetic Resonance

t_{obs} observation time

ThT Thioflavin T

TOF MS time-of-flight mass spectrometry

UV Ultra Violet

WAXS Wide Angle X-ray Scattering

Prologue

This thesis focuses on the physical-chemical properties of the Amyloid-β (Aβ) peptide that is one of the causative agents of the incurable human neuro-degenerative disorder known as Alzheimer´s diseases (AD).

The aim of the thesis:

- develop a robust bottom-up approach for solubility investigations in vitro of Aβ variants for systematic investigations of intrinsic and extrinsic factors that can influence the aggregation equilibrium
- develop a strategy where small angle scattering methods can be used to investigate Aβ fibril structures at the equilibrium state

The Aβ variants of interest in this thesis:

- Aβ40 wt: the most abundant variant found in cerebrospinal fluid
- Aβ42 wt: present in the amyloid plaques in the brain of AD patient
- Aβ42 S26Q: a phosphomimic mutant to investigate the role of side chain size on fibril structure and aggregation

The five most important results and observations in this thesis:

- Microfluidic diffusional sizing (MDS) and mass spectrometry (MALDI-TOF/TOF) with isotope standard can be used to quantify the solubility of Aβ40 in pure buffer conditions
- The equilibrium solubility of recombinant Aβ40 peptide was found to be S=0.36 ± 0.15 µM in aqueous solution of 20 mM sodium phosphate buffer, pH 7.4 at 37 °C.
- Aβ40 wt, Aβ42 wt and Aβ42 S26Q fibrils obtained at equilibrium state are made by two filaments
- Aβ40 filaments are made by four monomers per plane rather than three, as shown by the small angle scattering studies
- Aβ42 S26Q fibril shows a reduced cross-section when compared to Aβ42 wild type

1 Introduction

1.1 Proteins: the good, the bad and the ugly

Proteins[1] are essential to life and in spite of their diverse biological functions, they belong to the same class of bio-polymers[2]. As a matter of fact, they are built from a variety of different combinations of the same 20 amino acids made by N, C, S, O and H atoms[3] (Figure 1.1 a). In cells, the ribosome[4] is the molecular machine that translates the information encoded in the genome into a poly-peptide chain and the amino acids are linked via amide bonds by chemical reactions between the N- and C- termini (Figure 1.1b). We refer to a protein, when the bio-polymer is made by more than 50 amino-acids, otherwise it is a peptide[5]. Alternatively, a protein can be defined as a poly-peptide chain which is folded and carries some biological function. Proteins for in vitro studies can be produced either recombinantly[6], via host cell expression or syntetically, via chemical reactions[7]. The advantage of working with recombinant proteins lies in the homogeneity of the amino acid sequence and in the possibility of selective isotope labelling of the atoms for structural studies[8]. Thus, if high-purity recombinant proteins can be obtained, the follow-up experiments have higher chance to be successful[9]. However, whether the protein is synthetic or recombinant one has to confront with the issue of protein folding[10], the physical process by which the poly-peptide chain assume a given three-dimensional structure. The protein fold is defined by the amino-acid sequence and the solution conditions. If protein folding goes awry, the resulting conformation causes problems that range from bad[11], if the protein loses its biological function, to ugly[12], when the protein self-assembles to form amyloid deposits[13] that impact human health. The latter case is observed for a class of bio-polymers[14] known as amyloid proteins[15] among which we find the Amyloid-β peptide (Aβ)[16](Figure 1.1c), which is involved

in Alzheimer's disease (AD) and is the focus of this thesis.

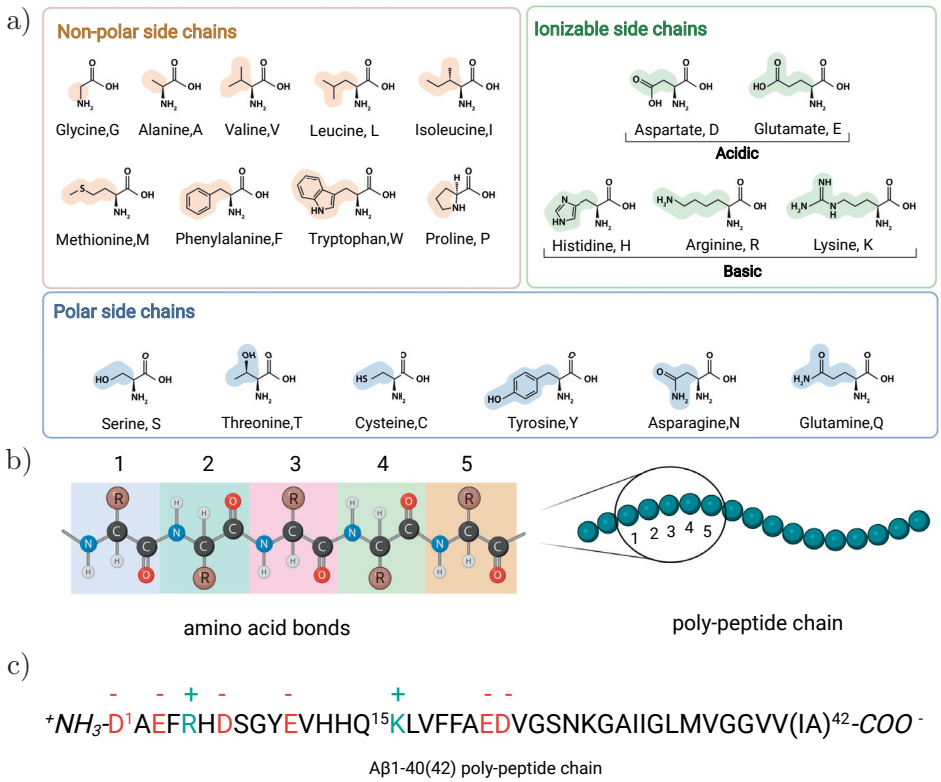

Figure 1.1 a) Reference chart showing the list of the twenty common amino acids coded from the human genome. b) Poly-peptide chain formed via chemical reaction of the carboxyl group and the amino group between adjacent amino acids. c) Amino acid sequence of Aβ40 and Aβ42 peptides.

1.2 Alzheimer's disease

Alzheimer's disease (AD)[17] is a cognitive and behavioural impairment caused by the initial damage of the human brain, which ultimately leads to organ dysfunctions and death. AD manifests as extracellular amyloid plaques mainly composed of abnormally folded amyloid-β (Aβ)[18] peptide and intracellular neurofibrillar tangles of tau protein[19] in the brain. AD usually does not affect people younger than 65 years old[20], unless it is caused by gene mutations passed from the parent to the child[21]. In the past century, the decline of the number of infectious diseases via more effective treatments greatly increased the life expectancy of the world population[22]

and so the aging threshold[23]. On the other hand, other factors might contribute to the increasing number of cases of AD in the modern world. Environmental conditions such as living in urban areas rather than close to nature can increase the exposure to polluting factors[24]. A sedentary lifestyle and lack of physical exercise[25], may also contribute to increased risk. Other co-factors may be sleep deprivation[26], cigarette smoking[27], a poor diet[28] and the presence of pre-existing metabolic or neuro-degenerative disorders[29,30]. Statistics carried on the USA population suffering from AD suggest a rise of cases from 5 to 135 million by 2050, making AD the new silent plague of our century[31](Figure 1.2).

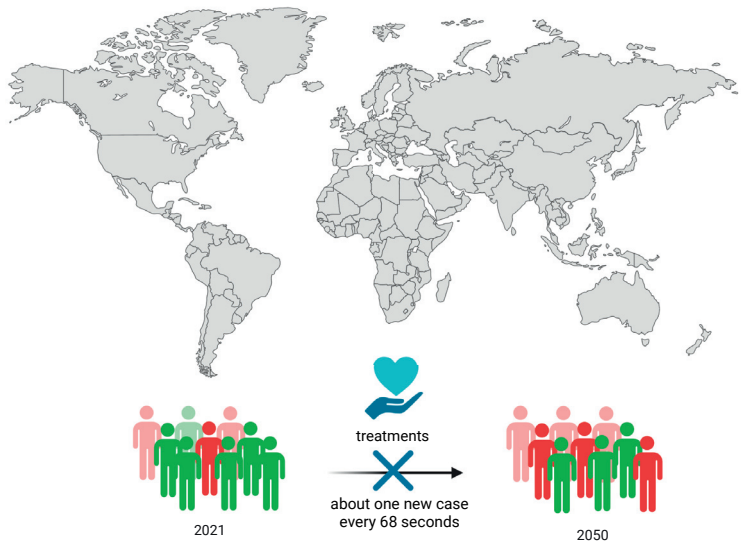

Figure 1.2 Alzheimer's disease worldwide forecasted to triple by 2050[31].

1.3 Amyloid-β: from monomer to fibril

Amyloid-β (Aβ) peptides[32] are produced in the brain of healthy individuals though the proteolytic activity of β-and γ-secretase enzymes towards the integral-membrane glycoprotein Amyloid Precursor Protein (APP)[2,33]. Depending on the cleavage position on the APP one can find Aβ variants with different length at the N- and C-terminus. Among them we find Aβ40 and 42, which differ by two amino acid residues (isoleucine and alanine) at the C-terminus[34]. While Aβ40 is the most abundant[35], the 42 residue variant is the most aggregation prone[36] and the main component of the fibrous

aggregates found in the brains of AD patients. Aβ can form, other than fibrils, aggregates distributed over a fairly large molecular weight range such as dimers, trimers, tetrameters up to larger globular assemblies generally called oligomers. Those are mainly hydrophobic and soluble. While the fibrillar aggregates seem to be the obvious pathological hallmark of AD they are relatively harmless compared to the oligomeric forms[37,38]. Thus, the latter can give rise to cellular toxicity through different mechanisms. Fibril formation can be monitored via thioflavin T (ThT)[39], which is an amyloid-specific dye that increases its fluorescence quantum yield upon binding to fibril. Studies of Aβ42 fibril formation, monitored by ThT fluorescence and isotope tracking experiments, have lead to the identification of three main steps of fibril formation[40]: primary nucleation, secondary nucleation and elongation. The aggregation process begins when the conditions for the primary nucleation are attained[41]. In supersaturated conditions[42], the formation of a critical nucleus of Aβ peptides with optimal size will trigger a transition from a monomer phase to a fibril phase (Figure 1.3a) as we discuss further in **Paper I**. Monomers can be added by the elongation step to the fibrils and take on their structure. The secondary nucleation step is the step that mainly contributes to the proliferation of oligomers via surface catalysis of monomers into new fibrils[43](Figure 1.3b). Recently it has been shown in vitro that nucleation at the fibril surface is stereospecific[44] and that the seeding by pre-formed fibrils is possible only for peptides that can form fibrils of the same structure as the seeds[45] (**Paper IV**). Kinetic studies give insight into the rate constants of the microscopic steps[46], however, does not reveal any structural information of the states formed during the aggregation pathway. In 2021, the U.S. Food and Drug Administration (FDA) approved the first monoclonal antibody called Aducanumab (Aduhelm™) as a treatment agent against mild forms of AD. Aducanumab shows the ability to target the modified aggregated forms of Aβ fibrils, reduce the amount of amlyoid plaques[47,48] and inhibits nucleation on the fibril surface[9]. These unique results highlight the importance of a better understanding of Aβ fibril structures for the design of inhibitors that bind to fibrils. However, while the solid-state nuclear magnetic resonance (ss-NMR) structure obtained for recombinant Aβ42 filaments was confirmed by independent studies carried out in parallel[49,50], up to now, a wide discrepancy has been observed between the ss-NMR structures of Aβ40 filaments[51-54] (**Paper III**). Another layer of complexity is added by the presence of different fibril structures obtained by the same Aβ variant, reported in literature as polymorphs[55]. Small angle scattering data in combination with the ss-NMR structures of the recombinant Aβ40 and

42 filaments, revealed in each case a detailed fibril model made by two filaments, fours monomers per plane (Figure 1.3c, **Paper II, III**). The molecular organization of different Aβ variants can provide insight of the thermodynamic fingerprint of the most stable aggregates at given experimental conditions. As a consequence, revealing the fibril structure of Aβ peptides under equilibrium conditions (**Paper II, III, IV**) might help to correlate the solubility concentrations of variants (**Paper I**) to their aggregation propensities[56].

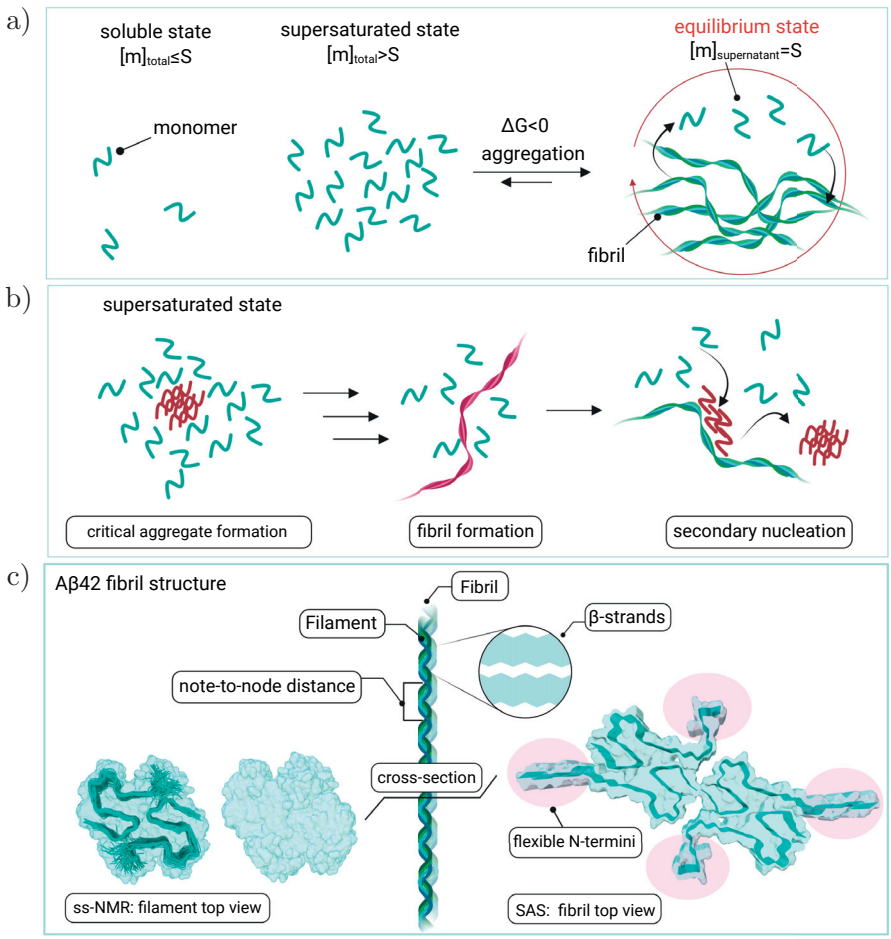

Figure 1.3 Schematic representations of a) the phase transition from a monomer phase to a fibril phase in Aβ42 aggregation. b) Secondary nucleation step at the surface of a pre-formed fibril. c) Aβ42 filament and fibril structures obtained by solid-state nuclear magnetic resonance spectroscopy (ss-NMR) and small angle scattering (SAS) methods.

2 Protein folding versus Fibril formation

2.1 Protein folds

The unique functional conformation of a protein, called native state, is characterised by four levels of protein structure: primary, secondary, tertiary and quaternary structure[57](Figure 2.1). The **primary structure** represents the unique amino acid sequence of a protein and determines its physical-chemical properties in solution. The **secondary structure** describes the arrangement of the backbone of the polypeptide chain. As a consequence of the hydrophobic effect, which governs the tertiary structure and thereby the assembly of secondary structure motifs, the poly-peptide either bends and folds (β-strand: parallel or anti-parallel) or spirals around (helices: $\alpha, 3_{10}$ or π). Those two motifs show a significant rigidity due to the formation of hydrogen bonds between amide hydrogens (N–H) and carbonyl oxygens (C=O) of the peptide backbones. The β-strand motif can, in turn, be associated by the main chain via hydrogen bonding interactions to form β-sheets between different segments of the polypeptide. The **tertiary structure** represents the overall fold of the protein, where different secondary structures are packed together giving the protein its unique three dimensional structure. Many globular proteins have a very dense packing where the hydrophobic parts of the molecule are shielded from water. Thus, the formation of the secondary and ternary structures is generally driven by the hydrophobic interactions and is a way to prevent hydrophobic amino acid side chains from contact with water. However, it may also involve specific interactions between particular amino acid side-chains that are polar. We note that the folding of a protein, where many of its hydrophobic residues are shielded from water, typically significantly

rises its solubility in water if compared to its unfolded or denaturated state. There is an analogy in surfactant micelle formation. Micelle formation at the critical micellization concentration effectively increases the surfactant solubility[58]. Finally, two or more folded polypeptide chains may associate, forming a super-molecular structure that is referred to as the **quaternary structure**.

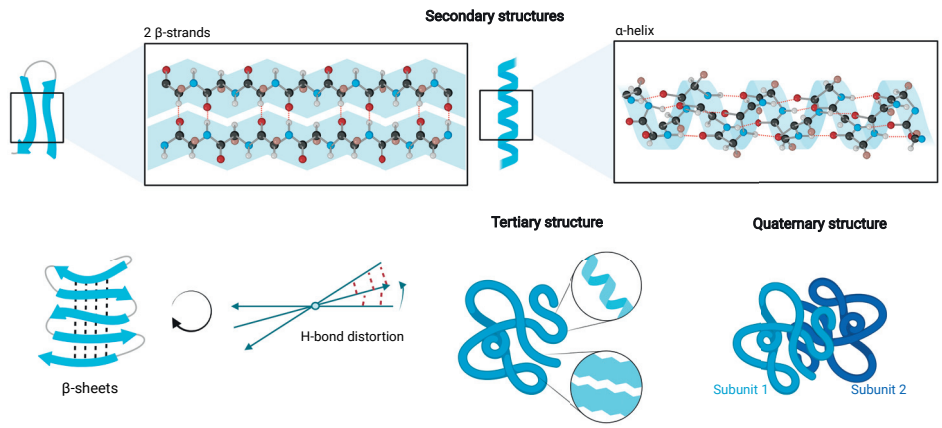

Figure 2.1 Schematic representation of the four levels of proteins structure.

2.2 Aβ as an intrinsically disordered peptide

The Aβ peptide is an intrinsically disordered peptide (IDP) meaning that it is lacking any secondary and tertiary structure in its native state. Thus, it behaves mainly as a random coil in solution. The contour length, i.e. the maximum extended chain length, L, of a protein, is given by $L = n_{aa} \cdot d_{aa}$, where n_{aa} is the number of amino acid in the polypeptide chain and $d_{aa} = 3,5$ Å the amino acid residue backbone dimension when stretched out on a plane. For the Aβ40 peptide, the contour length $L_{A\beta 40} = 15$ nm. In **Paper I**, the hydrodynamic radius, R_H, of Aβ40 monomers was found to be $\simeq 1.8$ nm, consistent with a random coil conformation in solution. From the theory of flexible polymers[59] we have that $R_H \approx 0.4(\lambda_p \cdot L)^{(1/2)}$, where $\lambda_p \approx 1$ nm[60] is the typical persistence length of a peptide chain[60,61]. With $\lambda_p \approx 1$ nm and $L = 15$ nm we thus expect $R_H \approx 1.6$ nm in good agreement with the experimental result.

2.3 Aβ folding as a fibril formation

The Aβ40 peptide has a very low aqueous solubility. In **Paper I** we found the solubility, S, to be $S = 0.36 \pm 0.15$ µM in aqueous solution of 20 mM sodium phosphate buffer at pH = 7.4 and $T = 37$ °C. The peptide is indeed very hydrophobic, but it is apparently unable to fold into a more water soluble structure. Instead we observe the formation of aggregates exhibiting a fibrillar structure. Thus, fibril formation can be seen as a folding phenomenon. Intrinsically disordered proteins such as Aβ, while behaving as a random coil in solution expose the hydrophobic residues to the water solvent. At this point hydrophobic interactions become predominant and Aβ peptides fold and self-assembles into a relative rigid and well-organised β-sheet rich structure. The coupled folding and self-assembly follows a nucleation-dependent polymerization model[40] and leads to the formation of the most thermodynamically stable state.

2.4 The free energy landscape of Aβ folds

Fibril formation can involve a complex free energy landscape (Figure 2.2a), with several metastable states in addition to the global free energy minimum[24,40,41,62-65]. The possible toxicity of small oligomer species has been extensively discussed[24,40,41,65]. There may also be a polymorphism in the mature fibril state with different possible structures[66]. Thus, there may be several possibilities for the system to get kinetically trapped in a metastable state.

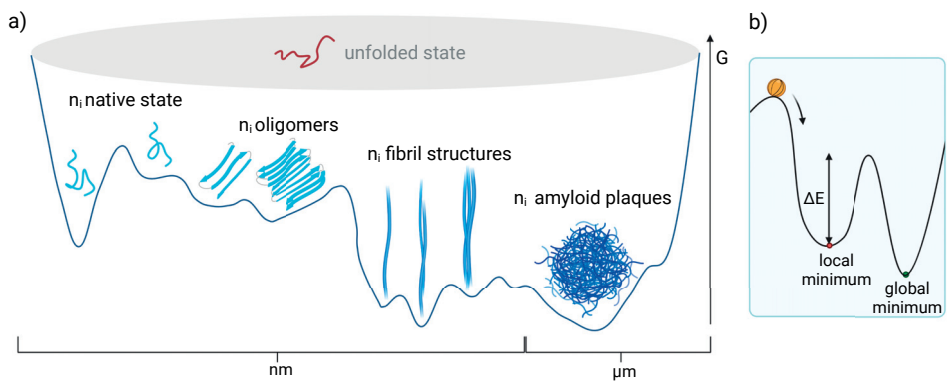

Figure 2.2 Schematic representation of a) the energy landscape of Aβ conformations, b) the local and global minimum.

As an example, let us take a basketball rolling down hill with a kinetic energy given by $E_k = mv^2/2$, where m is the mass of the basketball and v its velocity (Figure 2.2b). In order to roll over another hill, the basketball needs to gain a kinetic energy which is higher than $\Delta E_p = mgh$, where g is the acceleration due to gravity and h is the height of the second hill. On the other hand, if E_k is lower then ΔE_p, the basketball is kinetically trapped in the gap between two hills. A similar scenario can describe the formation of intermediates in Aβ fibril formation. In the present thesis we have mainly focused on the state of mature fibrils of Aβ42 and Aβ40 at long times. Here, results of different experiments were very similar, indicating the presence of a single dominating fibril morphology (Chapter 5).

3 Driving forces in the self-assembly process

In the case of proteins and protein fibrils, the two most important interactions, both on the molecular length scale and the aggregate (colloidal length scale) level are the hydrophobic interactions and electrostatic interactions. Below we describe them briefly one by one[58,67].

3.1 Hydrophobic effect

The insolubility of non-polar molecules, like hydrocarbons, in water is generally referred to as the hydrophobic effect, and the clustering of such molecules when exposed to water is said to be the result of hydrophobic interactions[58,68]. These non-polar molecules are characterized as being hydrophobic, in contrast to hydrophilic, and the insolubility is a consequence of water being a strongly hydrogen bonding solvent[69]. The transfer of an oil molecule from its neat phase into water is associated with a decrease in entropy resulting from the perturbation of water's three dimensional hydrogen bonding network, and an increased structuring of water molecules in the vicinity of the solute.

Biological life on Earth is based on water as the solvent, and many cellular structures and biological processes are consequences of the hydrophobic effect. An important example being the self-assembly of lipids into various membrane structures including the plasma membrane of our cells. It is well established that the hydrophobic interaction is also the dominating driving force for protein folding[70]. It is also considered to be the dominating driving force for protein fibrillation[71].

3.2 Electrostatic interactions

Protein molecules consist of a mixture of non-polar (hydrophobic), polar and charged residues. Hence, besides hydrophobic interaction we also need to consider electrostatic interactions. The charged residues involve amines and carboxyl groups that are titratable, and the protein net charge hence varies with pH. It typically goes from positive to negative with increasing pH, crossing zero at the isoelectric point. This has the implication for example that the Aβ40 monomer solubility, discussed in **Paper I**, is a property that may depend significantly on the pH. When the net charge is high, there is a strong electrostatic penalty for folding the chain and condensing the charges into a smaller volume. In a closely packed folded state, there may be favorable attractions between oppositely charged residuces and the formation of salt bridges[72].

Electrostatic interactions are also important on the colloidal length scale. Amyloid fibril are large colloidal objects, that moreover may still contain significant amounts hydrophobic patches on their surfaces. In order for the fibrils to be colloidally stable, they need to be charge stabilized, which requires a sufficient amount of surface charge. Otherwise, they will aggregate into dense fibril clusters[73].

4 Fibril formation as a phase transition

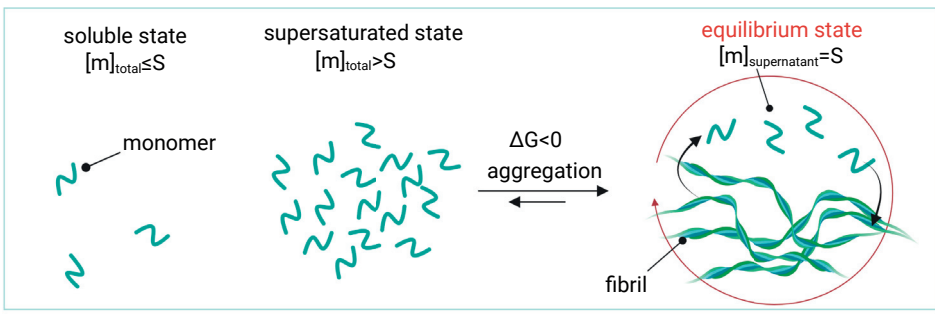

Unless there is complete miscibility over the whole range of compositions, a compound typically has a finite solubility, S, in a solvent. For supersaturated conditions, i.e. for concentrations $c > S$, the compound either precipitates as a solid phase or there is a liquid-liquid phase separation with coexisting concentrated and dilute solutions. In either case, there is at equilibrium a coexistence of two-phases (liquid-solid or liquid-liquid) with the compound being present in both (dilute and concentrated, respectively). Thermodynamic equilibrium corresponds to the state of the overall system that has the lowest free energy. In case of a two phase equilibrium, this implies that the chemical potential of a given component is the same in the two coexisting phases.

Fibril formation, as in the case of Aβ, can be viewed as the precipitation of a new phase[74] (fibril) from a supersaturated solution with $c > S$. This new phase is relatively ordered, and we can consider it as a solid (or semi-solid). Within this first order phase transition picture we expect, as fibrils are being

formed and grow, that the monomer concentration gradually decreases with time until an equilibrium is obtained, where the monomer concentration has become equal to S. Obviously, an accurate determination of S of an amyloid forming peptide is important, as it reports on the propensity of the peptide to aggregate.

4.1 Aβ solubility

In **Paper I** we have determined the solubility of Aβ40 at pH 7.4 at 37 °C. Under these conditions we found that $S = 0.36 \pm 0.15$ µM. In the phase transition picture outlined above, S corresponds to the concentration of monomers that at thermodynamic equilibrium coexist with fibrils. In the monomer solution phase, the peptide chemical potential can be written as

$$\mu_m = \mu_m^\circ + k_B T \ln(c) \tag{4.1}$$

where k_B is Boltzmann's constant and T is the absolute temperature and c is the concentration. The constant μ_m° is the monomer standard chemical potential in the solution phase that involves the nearest neighbor interactions with the solvent molecules. The second term results from the entropy of mixing. The fibril "phase" is semi-ordered, and there is no entropy of mixing term. Consequently, the peptide chemical potential in this "phase", μ_f, can be considered to be a constant that we can refer to as a fibril standard chemical potential, μ_f°. Thus,

$$\mu_f = \mu_f^\circ \tag{4.2}$$

At equilibrium, monomers at a certain concentration $c = S$ coexist with fibrils. From the equilibrium condition $\mu_m = \mu_f$ we have that

$$S = e^{\frac{\Delta\mu^\circ}{k_B T}} \tag{4.3}$$

where

$$\Delta\mu^\circ = \mu_f^\circ - \mu_m^\circ \tag{4.4}$$

The standard chemical potentials include the peptides' inter-molecular interactions with its environment, and the lower the standard chemical potential the more favorable is the environment. Hence, a low solubility, S, implies that peptide-peptide interactions in the fibrils are more favorable than the peptide-water interactions in the monomers' aqueous environment, and $\Delta\mu^\circ < 0$.

4.2 Kinetics vs thermodynamics

For $c > S$ the Aβ monomer solution is supersaturated and unstable relative to fibrils ($\mu_m > \mu_f$) that form **spontaneously**. However, the rate of formation can be low and the process may show a significant lag time, in particular at low supersaturations where μ_m is only slightly larger than μ_f. Associated with the lag time, one can identify a metastable zone as a range of supersaturation where the solutions are metastable, without any macroscopically observable amount of fibrils being formed during a given observation time, t_{obs} [75]. This range decreases monotonically with increasing t_{obs} and approaches zero as t_{obs} goes to infinity. This can be understood within the framework of classical nucleation theory, which predicts that the rate of homogeneous primary nucleation approaches zero as c decreases to S[75,76]. For $c = S$ no nucleation should occur. The aggregation kinetics of a supersaturated solution of Aβ can be conveniently followed by ThT fluorescence[39]. A significant amount of systematic studies of Aβ fibril formation kinetics in recent years[36,43,77] have shown that apart from primary nucleation and growth (fibril elongation), there can also be a significant amount of secondary nucleation events occurring at already formed fibril surfaces. Also fibril fragmentation may contribute to the kinetics as it creates additional fibril ends where elongation can occur. Secondary nucleation is particularly important as its rate can be significantly higher than that of primary nucleation.

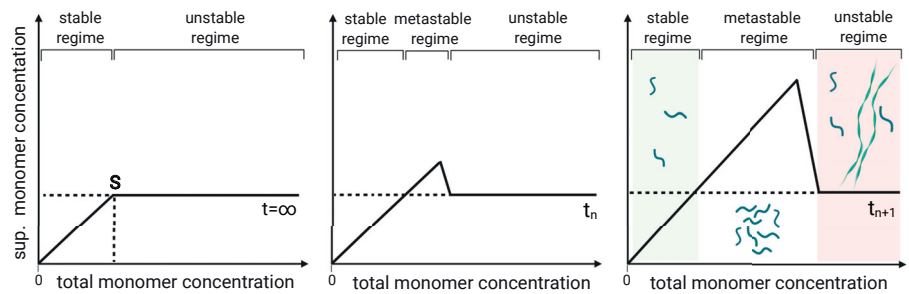

Figure 4.1 Schematic representation of the stable, metastable and unstable regimes observed in the solubility studies of Aβ40.

4.3 External factors in solubility studies

An accurate measurement of amyloid peptide solubility, as well as the range of the metastable zone, requires careful sample handling, freshly purified material and a systematic and reproducible approach with methods sensitive to concentrations in the picomolar range. In **Paper I** we developed a methodology to measure the solubility of Aβ in pure buffer conditions, with controlled ionic strength, in the absence of mechanical agitation, and at fixed given temperature. After different observation times, t_{obs}, samples were centrifuged to remove fibrils and the supernatant was investigated using a microfluidic diffusional sizing (MDS) technique that measures the hydrodynamic radius and also the peptide concentration using a fluorescent probe that binds to primary amines. In addition, monomer concentrations were measured using mass spectrometry with isotope standard.

4.3.1 Surface adsorption

In the Aβ solubility studies we are typically working with low sample volumes, meaning a relatively large interfacial area to volume ratio, and also low concentrations. To minimize surface adsorption low binding tubes were used in the solubility study. However, it is still useful to estimate the fraction of molecules in solutions which adsorb at the interface in the worst-case scenario, for example as a dense monolayer. Assuming for simplicity a spherical shape of a low binding tube, a volume of V=70 μL has an interfacial area of $A = 8 \cdot 10^{-5} m^2$. As discussed in **Paper I**, the monomer hydrodynamic radius of Aβ40 is $R_H \simeq 1.8$ nm and the radius of gyration of a random coil conformation can be estimated to $R_g \simeq 1.5$. If we further assume that the peptide monomers adsorb as a monolayer at the interface with an effective molecular cross-section area of $a \simeq \pi R_g^2 \simeq 7nm^2$, we can calculate the number, n, of adsorbed peptide molecules when the interface is fully covered and saturated as $n = A/a \simeq 1 \cdot 10^{13}$. The number of adsorbed peptide molecules can then be compared to the total number of peptide molecules in the sample volume, $n_{tot} \simeq cVN_A$ where c is the peptide molar concentration and N_A is Avogadro's number. With $c = 1$ µM and $V = 70$ µL, we obtain $n_{tot} = 4 \cdot 10^{13}$, demonstrating the absolute necessity of using low binding tubes for these kinds of studies.

4.3.2 Does the presence of the probe dye thioflavin T influence the Aβ solubility?

Fluorescent probes have been used over the last decade for mechanistic studies and rate constant determination of Aβ monomer aggregation, and among them thioflavin T (ThT) is the most common one. Probes for indirectly measuring different properties should always be used with great care. A relevant question, for example, is whether the presence of ThT influences the solubility of Aβ, and if so, how much. As ThT spontaneously binds to Aβ fibrils, it has the ability in principle to lower μ_f°, and thereby S. This reasoning, however, is complicated by the fact that ThT may also interact with Aβ monomers, although this is not detected in the fluorescence spectrum (no effect on the dye's quantum yield).

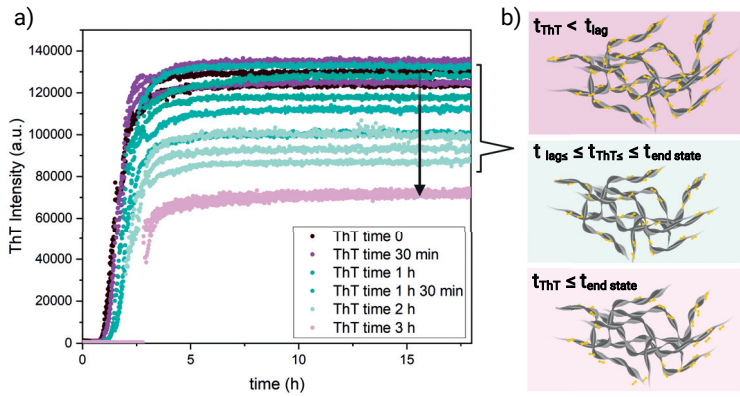

Figure 4.2 a) Aggregation kinetic experiment of 20 μM Aβ40 peptide in phosphate buffer solutions at pH 7.4 when ThT (100 μM) is added at time 0, 30 min, 1 h, 1 h 30 min, 2 h, 3 h during the aggregation process. b) Schematic representation of the interactions between ThT molecules and fibrils when ThT is added at different stages of fibril formation.

In a first attempt to investigate possible effects of ThT on fibril formation kinetics, a set of samples each containing 20 μM Aβ40 in 20 mM phosphate buffer solutions at pH = 7.4, were followed by fluorescence measurements as a function of time, $I(t)$. To the different samples, the probe ThT (100 μM) was added at different time points during the kinetics experiment. The temperature was kept at 37 °C. Experiments where the dye was added at $t = 0$, $t = 30$ min, $t = 1$ h, $t = 1$ h 30 min, $t = 2$ h all showed the same $t_{lag} = 60$ min, as well as the full $I(t)$ curve after the addition of the dye. Furthermore, the signal observed upon addition of ThT after 3 h ($> t_{lag}$) confirms that fibrils indeed had formed, within this time, both in the absence and presence of the dye. No significant difference in the kinetics

could be observed in agreement to what has been observed for Aβ42, where the aggregation in quartz NMR tubes or quartz cuvettes is independent of whether ThT is present or not[78]. However, a clear trend is that the fluorescence intensity at the end state is lower when ThT is added after the lag time. This indicates that either there is a decrease in the quantum yield of the bound ThT molecules, or in the amount of molecules that bind or both (Figure 4.2,b). In case that the number of bound molecules is lower, this would imply that some binding sites on the fibrils are readily accessible only during the fibril formation process.

5 Hierarchical structure of Aβ fibril

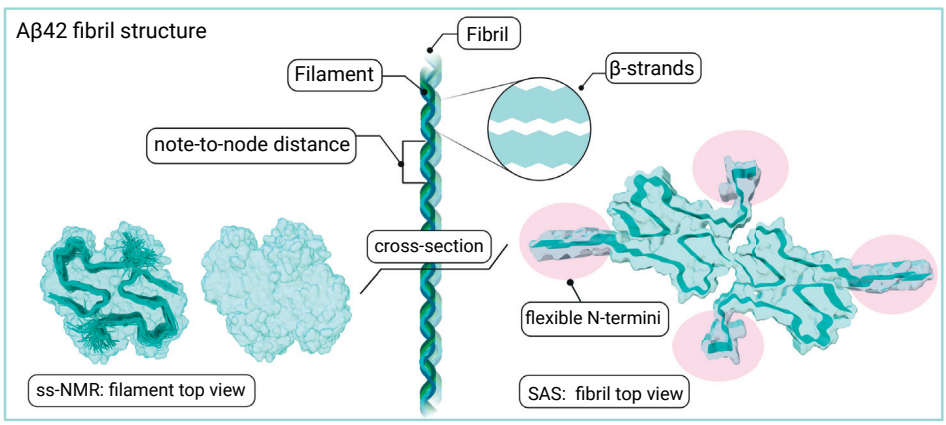

The structure of Aβ fibrils has been studied extensively over the years. Early X-ray fiber diffraction studies showed a characteristic cross-β pattern with sharp 4.7 Å meridian peaks and slightly broader 10 Å equatorial peaks[79]. Here, the 4.7 Å peak reports on the periodic β-strand separations in the intermolecular β-sheets that propagate in the fiber direction. We refer to this distance as d_β. The 10 Å peak corresponds to characteristic distance in the perpendicular direction although the exact interpretation of this peak is less clear.

More recently, solid state NMR (ss-NMR)[49,50,80] and cryo-EM[55,81,82] have provided fibril structures with essentially atomic resolution. However, the literature generally contains several different proposed structures for the same protein, including Aβ40 and 42. The reason for this can possibly be

attributed to different sample compositions, but it is also important to recall that these techniques involve major computations and proposed structures are selected on a probability basis and hence contain uncertainties. Following the tradition in structural biology, proposed structures[83] are generally uploaded to the Protein Data Base (PDB). In the present thesis we have investigated different Aβ fibril structures using small and wide angle X-ray scattering (SAXS and WAXS). In addition, some small angle neutron scattering (SANS) experiments were also performed. For the present fibril system, the SAXS patterns mainly report on the fibril cross-section shape and dimension, while the WAXS data confirm the presence of the $d_\beta = 4.7$ Å peak. In addition, we also compared our experimental data to model scattering calculations based on ss-NMR atomistic fibril structures (PDB ID: 5KK3).

5.1 Aβ42 cross-section and number of filaments

Aβ fibrils are generally very long (micrometer range)[84], and it is therefore not possible to measure the overall length with SAXS because this information lies outside the available q-range. We therefore focus mainly on the fibril cross-section in our analysis of the SAXS data, modelling the fibrils as elliptical rigid rods. When the fibril length is much longer than the smallest available q-value in the experiment, model scattered intensity can be written as

$$I(q) = \frac{C}{q}\, P_c(q) \tag{5.1}$$

where $P_c(q)$ is the normalized two dimensional cross-section form factor, and C is given by

$$C = \pi \Delta\rho^2 \phi \frac{V_p}{L} \tag{5.2}$$

Here, $\Delta\rho = \rho_p - \rho_b$ is the scattering length density difference between protein (p) and buffer (b), ϕ is the fibril (protein) volume fraction, and V_p/L is the protein volume per unit length in the fibrils. The scattering length densities are given by $\rho_p = 13 \cdot 10^{10}$ cm^{-2} and $\rho_w = 9.5 \cdot 10^{10}$ cm^{-2}, respectively. The normalized cross-section form factor of an elliptical cylinder can be written as

$$P_c(q) = \frac{2}{\pi} \int_0^{\pi/2} d\phi \left(\frac{2J_1(qr)}{(qr)} \right)^2 \tag{5.3}$$

where $J_1(x)$ is the first order Bessel function and

$$r = \left[(a\sin\phi)^2 + (b\sin\phi)^2\right]^{1/2} \tag{5.4}$$

In Figure 5.1. we present experimental SAXS data of two samples of Aβ42 fibrils, at pH = 7.4 and 8.0, respectively, together with the elliptical rod model scattering with the semi-axis $a = 3$ nm and $b = 9$ nm.

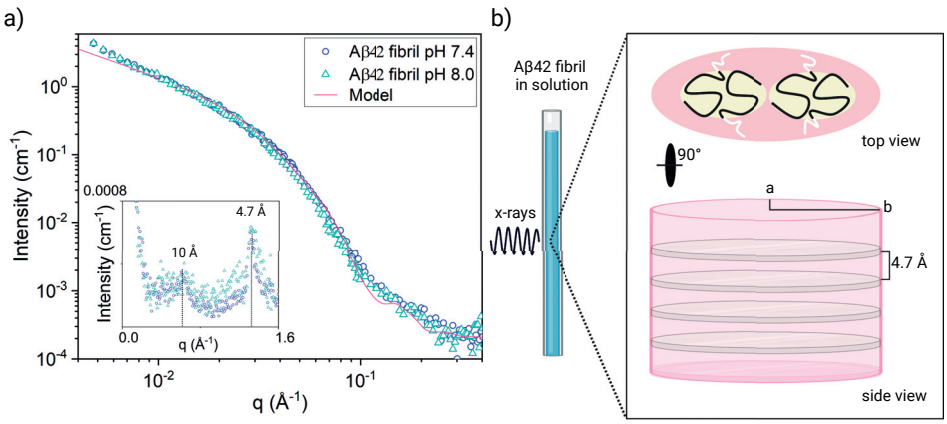

Figure 5.1 a) SAXS profiles of Aβ42 fibrils at pH 7.4 and 8.0. In the inset is reported the WAXS profile and the diffraction patterns at q = 0.6 and 1.3 Å^{-1}. b) Schematic representation of the elliptical cylinder model and the cross-section made by tetramer, two monomers per filament represented by the ss-NMR structure (PDB ID 5kk3).

As can be seen there is a good agreement between the model and data. The minor deviation in the q-range 0.1–0.3 Å^{-1} is due to the oscillations in the model form factor, which arise from the assumed sharp interface between the model elliptical cylinder and the solvent. In the real system, the fibril-solvent interface is expected to be more diffuse. A small deviation from the experimental data is also observed at the lowest q values. The slightly higher intensity observed in the experimental data compared to the model is likely due to some attractive fibril-fibril interactions. Similar effects were recently analyzed for α-synuclein fibrils, where it was shown that the intensity at these low q-values gradually increased as the pH was lowered towards the isoelectric point[85]. As an inset in Figure 5.1 is shown also the WAXS pattern. The $d_\beta = 2\pi/q = 4.7$ Å peak is clearly visible at $q = 1.3$ Å^{-1}, in addition to a broader hump, centered at $q = 0.6$ Å^{-1}, associated with the characteristic distance of 10 Å. In the fibril, the Aβ molecules are essentially folded in two dimensions. The folded molecules then stack in the third dimension with parallel β-sheets forming the fibril.

From ss-NMR it was found that in the case of Aβ42 fibrils there are two parallel stacks of molecules, as shown in the PDB structure presented in Figure 5.2.

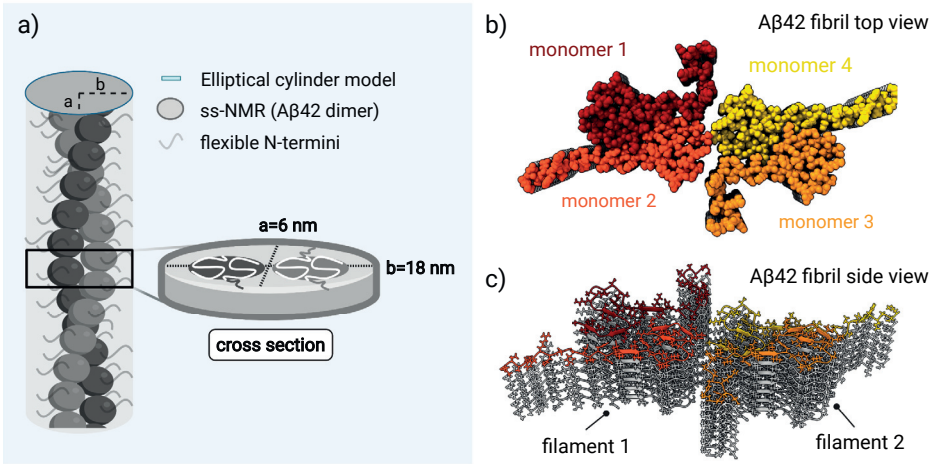

Figure 5.2 a) Schematic representation of Aβ42 fibril cross-section made by two filaments as suggested by the elliptical cylinder model. b) Aβ42 fibril made by four monomers per plane c) β-strand propagation along Aβ42 fibril axis.

Here it is shown that the two parallel stacks make up one filament. Because the SAXS data were recorded on absolute intensity scale, and we know the peptide concentration and the contrast, $\Delta\rho$, we are able to determine the peptide volume per unit length, Vp/L, from the experimental intensity (Eq. 5.2). From this value we are then further able to determine the number of filaments, N, in the fibrils by considering

$$V(p)/L = 2\frac{N v_{\mathrm{p}}}{d_{\beta}} \tag{5.5}$$

where v_p is the Aβ42 molecular volume.

The model calculation shown in Figure 5.1 corresponds to $N = 2$. In other words, the experimental data are consistent with the fibril being composed of 2 filaments, and thus 4 molecular stacks. The ss-NMR describe only one filament and not two, becasue the two filaments are not sufficiently close in space to give rise to cross peaks in the NMR spectrum. We have further investigated Aβ42 fibrils formed in the presence of the dye ThT (**Paper II**), as well as fibrils of the Aβ42 mutant S26Q (**Paper IV**). Data from these fibrils are also consistent with $N = 2$.

Table 5.1 Parameter values used in the modeling of the SAXS data.

Parameter	Aβ42	S26Q	Aβ42+ThT
protein concentration [μM]	350	350	350
molar weight [g/moL]	4645	4684	4645
protein mass density [g/mL]	1.43	1.43	1.43
background [cm^{-1}]	$2e^{-4}$	$2e^{-4}$	$2e^{-4}$
water (solvent) SLD [cm^{-2}]	$9.47e^{10}$	$9.47e^{10}$	$9.47e^{10}$
protein SLD [cm^{-2}]	$12.7e^{10}$	$12.7e^{10}$	$12.7e^{10}$
β-sheet repeat distance [Å]	4.7	4.7	4.7
N, number of filaments	2	2	2
semi-axis 1 ("radius") [nm]	3	2.7	3
semi-axis 2 ("radius") [nm]	9	8	9

In Table 5.1 we have summarized the parameter values used in the modelling of the SAXS data.

While no significant changes are observed for the fibril cross-section when binding ThT molecules, a slightly more compact packing of the two filaments is indicated for fibrils after mutation of serine to glutamine at position 26. The SAXS patterns from Aβ42 fibrils formed in the absence and presence of ThT (1:1 molar ratio) are compared in Figure 5.3. As an inset it is also shown the WAXS patterns.

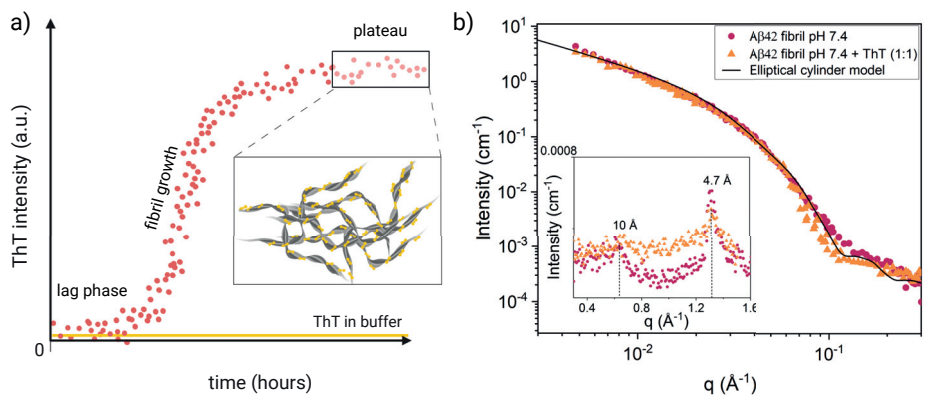

Figure 5.3 a) Schematic representation of the aggregation kinetic curve obtained when following Aβ42 aggregation with ThT fluorescence. The plateau corresponds to the end state of fibril formation b) SAXS-WAXS pattern of mature Aβ42 fibril (350 μM total concentration) obtained without and in the presence of ThT (1:1 molar ratio) during fibril formation.

The purpose of this experiment was to investigate whether the presence of ThT had any visible influence on the fibril structure. However, the fibril cross-section dimension and number of filaments appear to be the same in the presence of ThT. Also, the periodic β-sheet repeat distance, $d_\beta = 4.7$ Å, remains unchanged. In Figure 5.4 the experimental SAXS pattern from fibrils of the S26Q mutant is compared to that of the wild type (wt) fibrils.

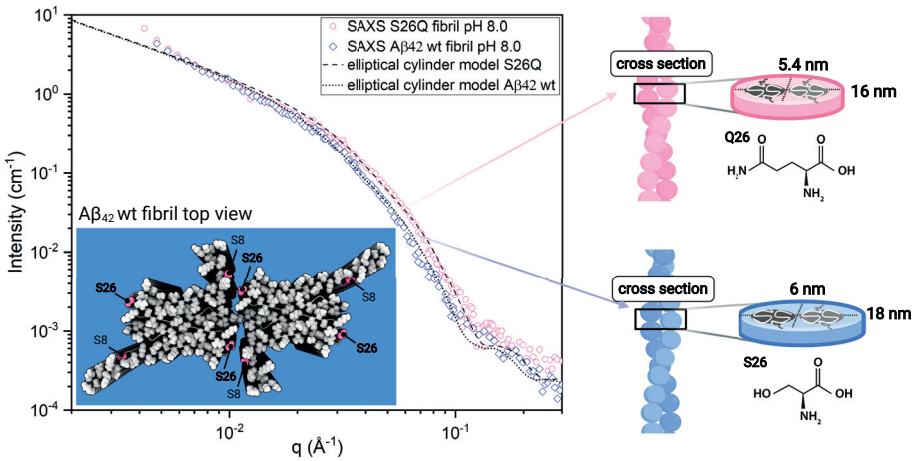

Figure 5.4 Left) Comparison of the SAXS patterns from wt Aβ42 fibrils (blue) and fibrils from the Aβ42 mutant S26Q (pink). In the insert we show the atomic structure of Aβ42 fibril. In pink colour is indicated the position of the serine group. Right) The slightly different fibril cross sections are illustrated.

The slightly smaller cross-section dimensions in the case of S26Q is clearly seen from the data. However, the data are still consistent with $N = 2$. The difference in cross-section dimension, between Aβ42 and S26Q, is probably due to a slightly closer packing of the two filaments for the mutated peptide.

5.2 Aβ40 fibril structure

Aβ40 is the most abundant Aβ variant found in cerebrospinal fluid (CSF) of healthy individuals. Intriguingly, Aβ40 shows a higher solubility and lower aggregation propensity when compared to Aβ42 (**Paper I**).

The cross-section shape and dimension of Aβ40 fibrils were investigated by SAXS in **Paper III**. In Figure 5.5. it is compared the SAXS patterns of

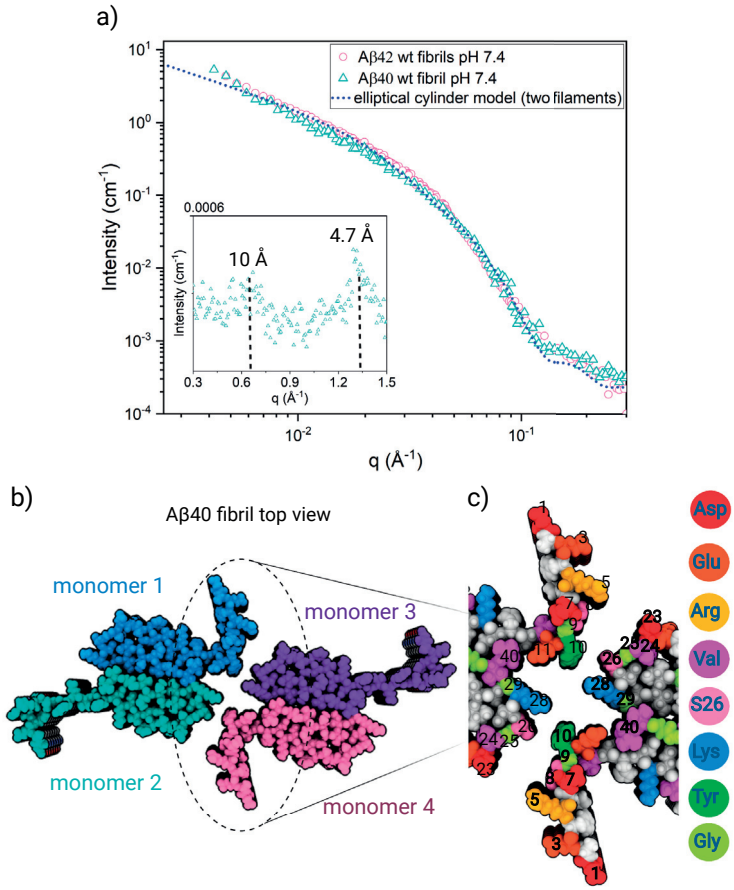

Figure 5.5 a) SAXS-WAXS patterns of Aβ40 and Aβ42 fibrils at pH 7.4. The dotted line is the model calculation for an elliptical cross-section with N=2. b) Zoom of Aβ40 fibril core showing the amino acid residues of contact between filament 1 and 2.

Aβ40 and Aβ42.

As can be seen, the patterns are very similar meaning that the Aβ40 and Aβ42 fibril cross-sections are very similar. We thus conclude that Aβ40 fibrils also are built up by 2 filaments and with an elliptical cross-section with semi-axis minor $a = 2.7$ nm and major $b = 10$ nm, respectively.

5.3 Considerations about Aβ morphs

In all our SAXS experiments on Aβ42 as well as Aβ40 fibrils we observe very minor differences in the fibril cross-section dimensions, indicating very similar molecular packing in the fibrils. Moreover, in the SAXS investigations of the S26Q Aβ42 variant fibril cross-section, it was found that the SAXS pattern obtained after 3 months was identical to the pattern obtained for 5 days old fibrils (**Paper IV**). Hence, no change is observed with time. Thus $N = 2$ appears to be a robust observation representing a deep free energy minimum, with negligible polymorphism with respect to this parameter. We note, however, that fibrils with different cross-section dimensions, possibly representing different morphs, have been reported in the literature[51,55,62,66,86].

6 Material and Methods

6.1 Sample preparation

Amyloid peptides require careful handling because of their strong tendency to aggregate. In the past, lack of control over sample preparation has led to incomparable experimental results between distinct scientific teams. Aβ40 (**Paper I, III**) and 42 (**Paper II**) used in this project, including the mutant S26Q (**Paper IV**), were expressed in Escherichia coli and purified from inclusion bodies[9]. The last step of Aβ purification is represented by the monomer isolation via **Size-Exclusion Chromatography (SEC)**. The sample travels across a stationary phase made by porous beads. The size separation depends on the protein Stokes radius. Thus, the smaller the protein is, the longer it will be retained in the gel´s pores. On the contrary, the larger protein size, the faster it will pass trough the gel phase (Figure 6.1.).

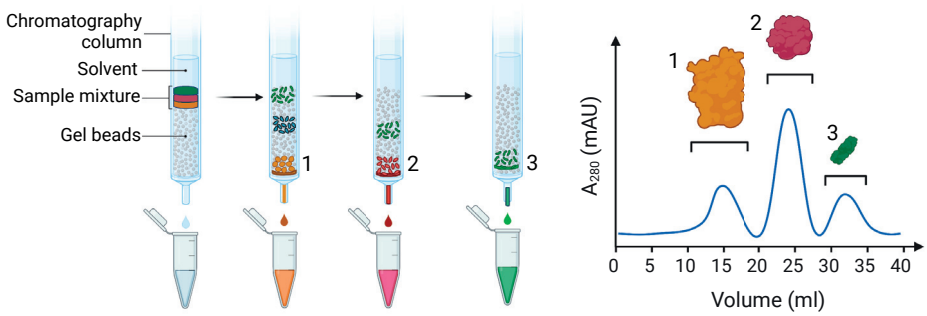

Figure 6.1 Schematic representation; Left) of a Size Exclusion Chromatography (SEC) on a sample containing proteins 1, 2 and 3; Right) chromatogram showing the elution volume of each protein.

6.1.1 Solubility studies

Freshly isolated Aβ40 monomer solutions are prepared by SEC and immediately dispensed at 4 °C in a 96-well plate (Corning® 3881, PEGylated polystyrene black plates with half-area wells) using a dispenser robot constructed in-house to retain precision and accuracy for small volume dilutions. The reproducibility of the dispenser robot has been validated by a dilution series of a pH-sensitive pyranine fluorescent dye[87]. The concentration of the dilution series is measured with microfluidic diffusional sizing and plotted versus the values obtained from the integrated absorbance at 280 nm of the SEC fraction collected to confirm the consistency of the methods with one another. Each sample of Aβ40 monomer is then individually transferred to low-binding tubes (MCT-150-L-C, Axygen, California, USA) of polypropylene and incubated at 37 °C at quiescent conditions for a given time. Monomer samples were not incubated for time longer than one week to avoid peptide proteolysis. Supernatant samples of Aβ40 are obtained after centrifugation (using a Hettich MIKRO 220/220 R centrifuge, rotor Cat. No. 1195-A) at 22640 g-force for 15 min at 37 °C[74]. A total volume of 70 µL for each monomer concentration is centrifuged at each specific time point and 25 µL are retrieved from the top of the sample in order to characterize the supernatant at different stages of the aggregation reaction without contamination by the sedimented fibrils.

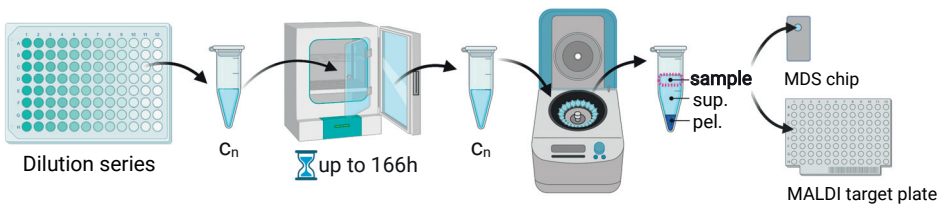

Figure 6.2 Schematic representation of the protocol used to prepared the samples for the solubility studies of Aβ40.

6.1.2 X-ray scattering studies

Aβ aliquots were dissolved in 1 ml of 6 M GuHCl at pH 8.4 and the sample injected on an Increase 10/300 GL (GE Healthcare) SEC column with a flow rate of 0.7 ml/min and eluted in 20 mM ammonium acetate, pH 8.5. Aβ fractions were lyophilized and the powder was dissolved in 20 mM sodium

phosphate, 0.2 mM EDTA, 0.02% NaN_3 at given pH at a final monomer concentration of 350 µM and a minimum volume of 250 µL. Aβ monomer samples were then incubated at 37 °C under quiescent conditions for 5 days to ensure aggregation end state. Aβ42 S26Q monomer samples were also incubated for 3 months to study structure variation over time.

6.1.3 Neutron scattering studies

Samples are prepared in the same way as for the SAXS experiments and carried to the neutron facility site at room temperature. Before the SANS experiment, a washing procedure is used to change the buffer to fully deuterated D_2O buffer, for a maximum contrast between protein and solvent. The pD of the deuterated phosphate buffer corresponds to the reading of the pH meter. The washing procedure is performed by centrifugation (using a Hettich MIKRO 220/220 R centrifuge, rotor Cat. No. 1195-A) at 22640 g-force for 20 min at r.t. and the supernatant is carefully retrieved without altering the fibril pellet at the bottom of the low-binding tube. The supernatant is replaced with fully deuterated buffer and between washing steps fibrils are re-dispersed by 30 s vortexing. In total 3 washing steps are executed, after which the buffer is added to obtain a final fibril concentration of 300 µM and a minimum volume of 450 µL.

6.2 Protein concentration determination by mass spectrometry (MALDI-TOF/TOF)

Mass spectrometry (MS) is an analytical method which allows the separation of ionised molecules based on their sizes and charges. When using the matrix assisted-desorption method (MALDI), the ionization source is a laser. The sample is mixed with a matrix which adsorbs the laser energy and transfers the protons to the protein molecules. In a time of flight experiment (TOF) an electric field is used to accelerate the ionised molecules. In this way, the ionised molecules are separated based on their ratio mass/charge (m/z) as a consequence of the time required for them to reach the detector. In order for the method to be quantitative, an internal standard with known concentration has to be used. In addition, the internal standard needs to have equivalent ionization properties of the protein of interest. In **Paper I**, the concentration for the supernatant of Aβ40 samples was determined by MALDI-TOF/TOF and ^{15}N isotope standard. For this purpose, ^{15}N-

incorporated Aβ(M1-42) peptide was expressed in M9 minimal medium containing $^{15}NH_4Cl$ as the sole nitrogen source. The peptide was purified as described[9] and monomers were isolated by SEC using a Superdex 75 Increase 10/300 GL (GE Healthcare) column in 20 mM sodium phosphate, 0.2 mM EDTA, 0.02% NaN_3 pH=8.0 In detail, 5 µL supernatant samples were digested after adding 5 µL ^{15}N-Aβ42 with one of two different stock concentrations. Samples were digested for 15 h with the Asp-N protease and then acidified with trifluoroacetic acid (TFA) to a final concentration of 0.5% to stop the proteolytic reaction. One µL sample was deposited together with 0.5 µL matrix, 5 mg/mL α-cyano-4-hydroxycinnamic acid (HCCA), on a ground steel plate and Pepmix II calibration standard (Bruker Daltronics) was used to externally calibrate the spectra. The Aβ-peptides derived from the normal ^{14}N supernatant samples and the isotope labelled ^{15}N protein samples are chemically identical and thus ionize identically. This can be used to compare and quantify the amount of protein in the sample. One of the peptides generated by the Asp-N digestion is MDAEFRH (amino acid M0 to H6) with a ^{14}N peptide mass of 905.39 Da and ^{15}N peptide mass of 917.39 Da (this peptide contains 12 nitrogen atoms). By comparing the total intensities of the signals in the isotope clusters for the two peptides (^{14}N and ^{15}N) the concentration of the Aβ40 in the supernatant samples can be determined.

6.3 Thioflavin T as optical probe for aggregation kinetics studies

Thioflavin T (ThT) it is a fluorophore, meaning that it is able to absorb light at a particular wavelength and then emit photons upon light excitation. In solution, the benzylamine and benzathiole rings of ThT rotate freely about their shared carbon-carbon bond. This rotation rapidly quenches excited states, causing low fluorescence emission for free ThT. In contrast, rotational immobilization of ThT in a "locked" state upon binding to amyloid fibrils leads to an enhancement of the quantum yield[39]. The aggregation kinetics on Aβ monomer samples are performed by using a plate reader (FLUOstar Omega, BMGLabtech) and the reading of ThT fluorescence occurs through the bottom of the plate (Corning® 3881, PEGylated polystyrene black plates with half-area wells) with excitation at 440 nm and using a 480 nm emission cut-off filter.

6.4 Microfluidic diffusional sizing (MDS) and concentration determination

The microfluidics diffusion sizing technology, MDS, uses a Fluidity One instrument, based on the interaction of an fluoraldehyd o-phthaldialdehyde (OPA) fluorogenic dye with the primary amines of the target species[88]. The ratio of the fluorescence in the two halves of the channel provides information about the average diffusion coefficient, D, while the sum provides the total peptide concentration. In detail, 5 µL of each supernatant sample is loaded in a disposable microfluidic chip made of cyclic olefin copolymer (COC) with a PEGylated-coated surface to minimize protein adhesion in the diffusion channel. The chip is made so that two streams can enter the same channel under laminar flow, i.e. with no convective mixing. The only way the protein can migrate from one half of the channel to the other half is by diffusion. Once the sample has travelled all the way through the channel, the flow is split again and the concentration is determined in each half of the channel after the interaction of OPA the primary amines. R_H, as measured by dynamic light scattering, is defined as the radius of an equivalent hard-sphere diffusing at the same rate as the molecule under observation. By MDS an apparent average hydrodynamic radius, R_H, for a spherical object, is obtained from the diffusion coefficient using the Stokes-Einstein relation.

6.5 Small angle scattering

Small angle scattering of X-rays (SAXS) and neutrons (SANS) are useful tools to investigate structures on the 1-100 nm length scale, and are extensively used to study e.g. colloidal particles and macromolecules in solution[89]. As the name suggests, the scattering from the sample is recorded at small angles. Sometimes, including in the present thesis, SAXS is complemented with the recording of scattering at wider angles (WAXS) to obtain information on the sub-nanometer length scale. The set-up of a typical SAXS or SANS experiment is illustrated in Figure 6.3.

A collimated beam of radiation impacts the sample and the scattering from the sample at different scattering angles, θ, is recorded with a two dimensional detector.

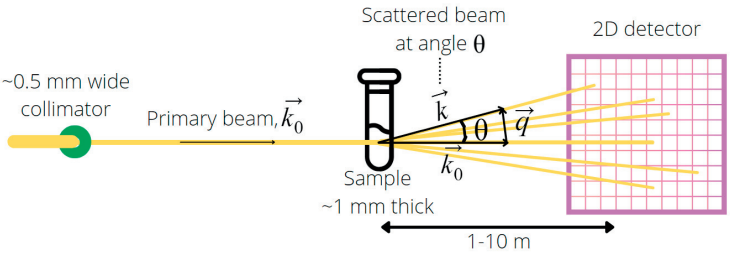

Figure 6.3 Schematic illustration of a small angle scattering set-up with scattering vectors of the primary and scattered beam and the scattering vector $\vec{q}$ indicated.

Denoting the wave vector of the primary beam $\vec{k_0}$ and that of the scattered wave $\vec{k}$, the difference is the so called scattering vector $\vec{q} = \vec{k} - \vec{k_0}$. The scattering events can be considered as purely elastic so that there is no exchange of energy. In this case the wave vector magnitude remains constant, $|\vec{k}| = 2\pi/\lambda$, where λ is the wavelength, and the scattering vector magnitude is given by

$$|\vec{q}| = q = \frac{4\pi}{\lambda} \sin\theta/2 \tag{6.1}$$

In the case of isotropic solutions, the scattering depends only on the magnitude of the scattering vector, and the scattering pattern on the two dimensional detector is circularly symmetric (Figure 6.4,a). It can then be convenient to radially average the data and plot the data in 1D as the scattered intensity $I(q)$ versus q (Figure 6.4,b).

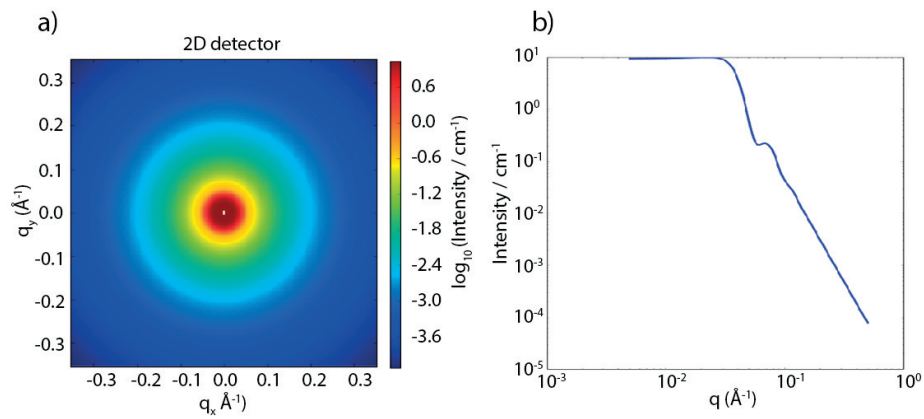

Figure 6.4 a) Schematic illustration of an isotropic two dimensional scattering pattern. b) Radially averaged one dimensional scattering pattern presented as $I(q)$ vs. q.

For a solution of identical particles, of volume fraction ϕ, the scattered intensity can be written as

$$I_P(q) = \phi V_P \Delta\rho^2 P(q) S(q). \tag{6.2}$$

Here, $\Delta\rho$ is the scattering contrast, which is the difference in the so-called scattering length density of the particles and the solvent, V_P is the particle volume, $P(q)$ is the single particle scattering function, the so-called form factor, and finally $S(q)$ is the so called structure factor, which reports on the relative positions of the particles. X-rays are scattered by the electrons of atoms and the scattering length density is proportional to the electron density. Neutrons are scattered by the atomic nuclei by a more complex interaction that can differ significantly also between isotopes, like normal hydrogen (H) and deuterium (D). This gives a particular advantage for neutron scattering as it allows for changing the scattering length density of for example a protein by replacing (H) with (D). For an aqueous (buffer) solvent it is particularly easy to vary the scattering length density by mixing H_2O and D_2O in different proportions. For a protein this is achieved by producing recombinant proteins in a D_2O environment. With these isotope exchanges it is possible to manipulate the contrast and in particular match the contrast between a given species and the solvent so that $\Delta\rho$=0, making the particles invisible. The single particle scattering function or form factor contains information of particle size and shape and is given by the square of a Fourier transform

$$P(\vec{q}) = \left| \int_{V_P} \mathrm{d}\vec{r} \exp(-i\vec{q} \cdot \vec{r}) \right|^2 \tag{6.3}$$

where the truncated Fourier integral is taken over the particle volume only (because $\Delta\rho$ is zero outside the particle). The structure factor $S(q)$ reports on the solution structure in the sense that depends on the relative positions of the particle. $1/q$ represents the typical length scale probed in the scattering experiments, and when typical particle distances are larger than $1/q$, one can make the approximation that $\Delta\rho = 0$.

The scattered intensity can be measured on an absolute scale, and is then usually presented in the unit of cm^{-1}. This is typically done by calibration with a known scatterer. For SAXS, the calibration is commonly done with H_2O, where the weak but measurable scattering in the small angle regime results from its density fluctuations with well known compressibility.

6.5.1 X-ray experiment

Each sample (150 µl) was loaded in a 1 mm-diameter quartz capillary. All measurements were made in an air-evacuated space at a pressure below 1.6 mbar and at room temperature and were performed using a Saxslab Ganesha pinhole instrument, JJ X-Ray System Aps (JJ X-ray, Hoersholm, Denmark) with an X-ray microsource (Xenocs, Sassenage, France) and a two-dimensional 300 k Pilatus detector (Dectris Ltd., Baden-Daettwil, Switzerland). The scattering experiments were performed with Cu K_α radiation having a wavelength, λ, of 1.54 Å. Samples were measured at three given sample-to-detector distances and the evolution of the scattering profile was monitored by data acquisition at different time points in order to detect possible fibril sedimentation. The 2D-images from the Pilatus detector were azimuthally averaged after subtracting the dark counts. The background, recorded in a capillary with buffer at the same contrast, was subtracted from the acquired 1D scattering data, $I(q)$.

6.5.2 Neutron experiment

SANS experiments were performed at the SANS-II instrument at the Swiss spallation source, SINQ, located at the Paul Scherrer Institute in Villigen, Switzerland. Demountable stainless steel cells were used and placed on a rotating rack to prevent precipitation. The sample was held in the cell between two quartz windows, each window sealed by an o-ring. The o-rings were compressed by retaining rings that were held down by four screws for a final sample thicknesses of 1 mm and sample minimum volume of 450 µL.

Bibliography

[1] Hartley, H. (1951) Origin of the Word 'Protein'. *Nature 168*, 244–244.

[2] Miller, S. L. (1953) A Production of Amino Acids Under Possible Primitive Earth Conditions. *Science 117*, 528–529.

[3] Dietzen, D. J. *Principles and Applications of Molecular Diagnostics*; Elsevier, 2018; pp 345–380.

[4] Pearson, H. (2001) Protein factory reveals internal works. *Nature* news010404–1.

[5] G. Storz, K. R., Y. I. Wolf (2014) Small Proteins Can No Longer Be Ignored. *Annual Review of Biochemistry 83*, 753–777.

[6] Structural Genomics Consortium,, Architecture et Fonction des Macromolécules Biologiques,, Berkeley Structural Genomics Center,, China Structural Genomics Consortium,, Integrated Center for Structure and Function Innovation,, Israel Structural Proteomics Center,, Joint Center for Structural Genomics,, Midwest Center for Structural Genomics,, New York Structural GenomiX Research Center for Structural Genomics,, Northeast Structural Genomics Consortium,, Oxford Protein Production Facility,, Protein Sample Production Facility, Max Delbrück Center for Molecular Medicine,, RIKEN Structural Genomics/Proteomics Initiative,, and SPINE2-Complexes, (2008) Protein production and purification. *Nature Methods 5*, 135–146.

[7] Bondalapati, S., Jbara, M., and Brik, A. (2016) Expanding the chemical toolbox for the synthesis of large and uniquely modified proteins. *Nature Chemistry 8*, 407–418.

[8] Tong, K. I., Yamamoto, M., and Tanaka, T. *Selective Isotope Labeling of Recombinant Proteins in Escherichia coli*; Springer New York, 2012; pp 439–448.

[9] Linse, S. *Expression and Purification of Intrinsically Disordered Aβ Peptide and Setup of Reproducible Aggregation Kinetics Experiment*; Springer US, 2020; pp 731–754.

[10] Dobson, C. M. (2001) The structural basis of protein folding and its links with human disease. *Philosophical Transactions of the Royal Society of London. Series B: Biological Sciences 356*, 133–145.

[11] J. M. Berg, L. S., J.L. Tymoczko *Protein Structure and Function - Biochemistry, 5th edition*; New York : W.H. Freeman, 2002.

[12] Chiti, F., and Dobson, C. M. (2017) Protein Misfolding, Amyloid Formation, and Human Disease: A Summary of Progress Over the Last Decade. *Annual Review of Biochemistry 86*, 27–68.

[13] Knowles, T. P. J., Vendruscolo, M., and Dobson, C. M. (2014) The amyloid state and its association with protein misfolding diseases. *Nature Reviews Molecular Cell Biology 15*, 384–396.

[14] Gallardo, R., Ranson, N. A., and Radford, S. E. (2020) Amyloid structures: much more than just a cross-β fold. *Current Opinion in Structural Biology 60*, 7–16.

[15] Ke, P. C., Zhou, R., Serpell, L. C., Riek, R., Knowles, T. P. J., Lashuel, H. A., Gazit, E., Hamley, I. W., Davis, T. P., Fändrich, M., Otzen, D. E., Chapman, M. R., Dobson, C. M., Eisenberg, D. S., and Mezzenga, R. (2020) Half a century of amyloids: past, present and future. *Chemical Society Reviews 49*, 5473–5509.

[16] Murphy, M. P., and LeVine, H. (2010) Alzheimer's Disease and the Amyloid-β Peptide. *Journal of Alzheimer's Disease 19*, 311–323.

[17] DeTure, M. A., and Dickson, D. W. (2019) The neuropathological diagnosis of Alzheimer's disease. *Molecular Neurodegeneration 14*, 32.

[18] Brookmeyer, R., Gray, S., and Kawas, C. (1998) Projections of Alzheimer's disease in the United States and the public health impact of delaying disease onset. *American Journal of Public Health 88*, 1337–1342.

[19] Hampel, H. et al. (2004) Measurement of Phosphorylated Tau Epitopes in the Differential Diagnosis of Alzheimer Disease. *Archives of General Psychiatry 61*, 95.

[20] Hou, Y., Dan, X., Babbar, M., Wei, Y., Hasselbalch, S. G., Croteau, D. L., and Bohr, V. A. (2019) Ageing as a risk factor for neurodegenerative disease. *Nature Reviews Neurology 15*, 565–581.

[21] Masters, C. L., Simms, G., Weinman, N. A., Multhaup, G., McDonald, B. L., and Beyreuther, K. (1985) Amyloid plaque core protein in Alzheimer disease and Down syndrome. *Proceedings of the National Academy of Sciences 82*, 4245–4249.

[22] Max Roser, H. R., and Ortiz-Ospina, E. (2013) World Population Growth. *Our World in Data* https://ourworldindata.org/world-population-growth.

[23] Dobson, C. M. (2015) Alzheimer's disease: addressing a twenty-first century plague. *Rendiconti Lincei 26*, 251–262.

[24] Zhou, M. et al. (2019) Mortality, morbidity, and risk factors in China and its provinces, 1990–2017: a systematic analysis for the Global Burden of Disease Study 2017. *The Lancet 394*, 1145–1158.

[25] Falck, R. S., Davis, J. C., and Liu-Ambrose, T. (2016) What is the association between sedentary behaviour and cognitive function? A systematic review. *British Journal of Sports Medicine 51*, 800–811.

[26] Winer, J. R., Mander, B. A., Helfrich, R. F., Maass, A., Harrison, T. M., Baker, S. L., Knight, R. T., Jagust, W. J., and Walker, M. P. (2019) Sleep as a Potential Biomarker of Tau and β-Amyloid Burden in the Human Brain. *The Journal of Neuroscience 39*, 6315–6324.

[27] Durazzo, T. C., Mattsson, N., Weiner, M. W., and Initiative, A. D. N. (2014) Smoking and increased Alzheimer's disease risk: A review of potential mechanisms. *Alzheimer's & Dementia 10*, S122–S145.

[28] Morris, M. C. (2009) The role of nutrition in Alzheimer's disease: epidemiological evidence. *European Journal of Neurology 16*, 1–7.

[29] Beydoun, M. A., Beydoun, H. A., and Wang, Y. (2008) Obesity and central obesity as risk factors for incident dementia and its subtypes: a systematic review and meta-analysis. *Obesity Reviews 9*, 204–218.

[30] Arvanitakis, Z., Wilson, R. S., Bienias, J. L., Evans, D. A., and Bennett, D. A. (2004) Diabetes Mellitus and Risk of Alzheimer Disease and Decline in Cognitive Function. *Archives of Neurology 61*, 661.

[31] Association, A. (2015) 2015 Alzheimer's disease facts and figures. *Alzheimer's & Dementia 11*, 332–384.

[32] Glenner, G. G., and Wong, C. W. (1984) Alzheimer's disease: Initial report of the purification and characterization of a novel cerebrovascular amyloid protein. *Biochemical and Biophysical Research Communications 120*, 885–890.

[33] Zheng, H., and Koo, E. H. (2011) Biology and pathophysiology of the amyloid precursor protein. *Molecular Neurodegeneration 6*, 27.

[34] Kummer, M. P., and Heneka, M. T. (2014) Truncated and modified amyloid-beta species. *Alzheimer's Research & Therapy 6*, 28.

[35] Portelius, E., Westman-Brinkmalm, A., Zetterberg, H., and Blennow, K. (2006) Determination of β-Amyloid Peptide Signatures in Cerebrospinal Fluid Using Immunoprecipitation-Mass Spectrometry. *Journal of Proteome Research 5*, 1010–1016.

[36] Meisl, G., Yang, X., Hellstrand, E., Frohm, B., Kirkegaard, J. B., Cohen, S. I. A., Dobson, C. M., Linse, S., and Knowles, T. P. J. (2014) Differences in nucleation behavior underlie the contrasting aggregation kinetics of the Aβ40 and Aβ42 peptides. *Proceedings of the National Academy of Sciences 111*, 9384–9389.

[37] Sengupta, U., Nilson, A. N., and Kayed, R. (2016) The Role of Amyloid-β Oligomers in Toxicity, Propagation, and Immunotherapy. *EBioMedicine 6*, 42–49.

[38] De, S. et al. (2019) Different soluble aggregates of Aβ42 can give rise to cellular toxicity through different mechanisms. *Nature Communications 10*.

[39] Naiki, H., Higuchi, K., Hosokawa, M., and Takeda, T. (1989) Fluorometric determination of amyloid fibrils in vitro using the fluorescent dye, thioflavine T. *Analytical Biochemistry 177*, 244–249.

[40] Cohen, S. I. A., Linse, S., Luheshi, L. M., Hellstrand, E., White, D. A., Rajah, L., Otzen, D. E., Vendruscolo, M., Dobson, C. M., and Knowles, T. P. J. (2013) Proliferation of amyloid- 42 aggregates occurs through a secondary nucleation mechanism. *Proceedings of the National Academy of Sciences 110*, 9758–9763.

[41] Cohen, S. I. A., Cukalevski, R., Michaels, T. C. T., Šarić, A., Törnquist, M., Vendruscolo, M., Dobson, C. M., Buell, A. K., Knowles, T. P. J., and Linse, S. (2018) Distinct thermodynamic signatures of oligomer generation in the aggregation of the amyloid-β peptide. *Nature Chemistry 10*, 523–531.

[42] Cellmer, T., Ferrone, F. A., and Eaton, W. A. (2016) Universality of supersaturation in protein-fiber formation. *Nature Structural & Molecular Biology 23*, 459–461.

[43] Törnquist, M., Michaels, T. C. T., Sanagavarapu, K., Yang, X., Meisl, G., Cohen, S. I. A., Knowles, T. P. J., and Linse, S. (2018) Secondary nucleation in amyloid formation. *Chemical Communications 54*, 8667–8684.

[44] Törnquist, M., and Linse, S. (2021) Chiral Selectivity of Secondary Nucleation in Amyloid Fibril Propagation. *Angewandte Chemie International Edition 60*, 24008–24011.

[45] Thacker, D., Sanagavarapu, K., Frohm, B., Meisl, G., Knowles, T. P. J., and Linse, S. (2020) The role of fibril structure and surface hydrophobicity in secondary nucleation of amyloid fibrils. *Proceedings of the National Academy of Sciences 117*, 25272–25283.

[46] Cohen, S. I., Vendruscolo, M., Dobson, C. M., and Knowles, T. P. (2012) From Macroscopic Measurements to Microscopic Mechanisms of Protein Aggregation. *Journal of Molecular Biology 421*, 160–171.

[47] Haeberlein, S. B. et al. Topline results from Phase 3 aducanumab studies. 2013; San Diego, CA.

[48] Sevigny, J. et al. (2016) The antibody aducanumab reduces Aβ plaques in Alzheimer's disease. *Nature 537*, 50–56.

[49] Wälti, M. A., Ravotti, F., Arai, H., Glabe, C. G., Wall, J. S., Böckmann, A., Güntert, P., Meier, B. H., and Riek, R. (2016) Atomic-resolution structure of a disease-relevant Aβ(1–42) amyloid fibril. *Proceedings of the National Academy of Sciences 113*, E4976–E4984.

[50] Colvin, M. T., Silvers, R., Ni, Q. Z., Can, T. V., Sergeyev, I., Rosay, M., Donovan, K. J., Michael, B., Wall, J., Linse, S., and Griffin, R. G. (2016) Atomic Resolution Structure of Monomorphic Aβ42 Amyloid Fibrils. *Journal of the American Chemical Society 138*, 9663–9674.

[51] Paravastu, A. K., Leapman, R. D., Yau, W.-M., and Tycko, R. (2008) Molecular structural basis for polymorphism in Alzheimer's -amyloid fibrils. *Proceedings of the National Academy of Sciences 105*, 18349–18354.

[52] Petkova, A. T., Ishii, Y., Balbach, J. J., Antzutkin, O. N., Leapman, R. D., Delaglio, F., and Tycko, R. (2002) A structural model for Alzheimer's -amyloid fibrils based on experimental constraints from solid state NMR. *Proceedings of the National Academy of Sciences 99*, 16742–16747.

[53] Petkova, A. T., Yau, W.-M., and Tycko, R. (2005) Experimental Constraints on Quaternary Structure in Alzheimer's β-Amyloid Fibrils. *Biochemistry 45*, 498–512.

[54] Bertini, I., Gonnelli, L., Luchinat, C., Mao, J., and Nesi, A. (2011) A New Structural Model of Aβ40 Fibrils. *Journal of the American Chemical Society 133*, 16013–16022.

[55] Kollmer, M., Close, W., Funk, L., Rasmussen, J., Bsoul, A., Schierhorn, A., Schmidt, M., Sigurdson, C. J., Jucker, M., and Fändrich, M. (2019) Cryo-EM structure and polymorphism of Aβ amyloid fibrils purified from Alzheimer's brain tissue. *Nature Communications 10*, 4760.

[56] K. Trainor, E. M., A. Broom (2017) Exploring the relationships between protein sequence, structure and solubility. *Current Opinion in Structural Biology 42*, 136–146.

[57] Schulz G. E., S. R. H. *Principles of Protein Structure*; Springer, 1985.

[58] Evans, D. F., and Wennerström, H. *The Colloidal Domain: Where Physics, Chemistry, Biology and Technology Meet. 2nd ed. Wiley-VCH*; New York, 1999.

[59] Richards, E. *An Introduction to Physical Properties of Large Molecules in Solution*; Cambridge University Press, 1980.

[60] Walther, K. A., Grater, F., Dougan, L., Badilla, C. L., Berne, B. J., and Fernandez, J. M. (2007) Signatures of hydrophobic collapse in extended proteins captured with force spectroscopy. *Proceedings of the National Academy of Sciences 104*, 7916–7921.

[61] Schlierf, M., Li, H., and Fernandez, J. M. (2004) The unfolding kinetics of ubiquitin captured with single-molecule force-clamp techniques. *Proceedings of the National Academy of Sciences 101*, 7299–7304.

[62] Adamcik, J., and Mezzenga, R. (2018) Amyloid Polymorphism in the Protein Folding and Aggregation Energy Landscape. *Angewandte Chemie International Edition 57*, 8370–8382.

[63] Abelein, A., Jarvet, J., Barth, A., Gräslund, A., and Danielsson, J. (2016) Ionic Strength Modulation of the Free Energy Landscape of Aβ40 Peptide Fibril Formation. *Journal of the American Chemical Society 138*, 6893–6902.

[64] Chen, M., Schafer, N. P., and Wolynes, P. G. (2018) Surveying the Energy Landscapes of Aβ Fibril Polymorphism. *The Journal of Physical Chemistry B 122*, 11414–11430.

[65] Bitan, G., Kirkitadze, M. D., Lomakin, A., Vollers, S. S., Benedek, G. B., and Teplow, D. B. (2003) Amyloid β-protein (Aβ) assembly: Aβ40 and Aβ42 oligomerize through distinct pathways. *Proceedings of the National Academy of Sciences 100*, 330–335.

[66] Aubrey, L. D., Blakeman, B. J. F., Lutter, L., Serpell, C. J., Tuite, M. F., Serpell, L. C., and Xue, W.-F. (2020) Quantification of amyloid fibril polymorphism by nano-morphometry reveals the individuality of filament assembly. *Communications Chemistry 3*, 125.

[67] Israelachvili, J. N. *Intermolecular and Surface Forces 3rd ed. Elsevier*; Waltham MA, USA, 2011.

[68] Southall, N. T., Dill, K. A., and Haymet, A. D. J. (2002) A View of the Hydrophobic Effect. *The Journal of Physical Chemistry B 106*, 521–533.

[69] Chandler, D. (2005) Interfaces and the driving force of hydrophobic assembly. *Nature 437*, 640–647.

[70] Tanford, C. (1997) How protein chemists learned about the hydrophobic factor. *Protein Science 6*, 1358–1366.

[71] van Gils, J. H. M., van Dijk, E., Peduzzo, A., Hofmann, A., Vettore, N., Schützmann, M. P., Groth, G., Mouhib, H., Otzen, D. E., Buell, A. K., and Abeln, S. (2020) The hydrophobic effect characterises the thermodynamic signature of amyloid fibril growth. *PLoS Computational Biology 16*, e1007767.

[72] Bosshard, H. R., Marti, D. N., and Jelesarov, I. (2004) Protein stabilization by salt bridges: concepts, experimental approaches and clarification of some misunderstandings. *Journal of Molecular Recognition 17*, 1–16.

[73] Dubackic, M., Idini, I., Lattanzi, V., Liu, Y., Martel, A., Terry, A., Haertlein, M., Devos, J. M., Jackson, A., Sparr, E., Linse, S., and Olsson, U. (2021) On the Cluster Formation of α-Synuclein Fibrils. *Frontiers in Molecular Biosciences 8, 768004*.

[74] Hellstrand, E., Boland, B., Walsh, D. M., and Linse, S. (2009) Amyloid β-Protein Aggregation Produces Highly Reproducible Kinetic Data and Occurs by a Two-Phase Process. *1*, 13–18.

[75] Lindfors, L., Forssén, S., Westergren, J., and Olsson, U. (2008) Nucleation and crystal growth in supersaturated solutions of a model drug. *Journal of Colloid and Interface Science 325*, 404–413.

[76] Kashchiev, D. *Nucleation: Basic Theory and Applications*; Oxford: Butterworth Heinemann, 2000.

[77] Yang, X., Meisl, G., Frohm, B., Thulin, E., Knowles, T. P. J., and Linse, S. (2018) On the role of sidechain size and charge in the aggregation of Aβ42 with familial mutations. *Proceedings of the National Academy of Sciences 115*, E5849–E5858.

[78] Törnquist, M., Cukalevski, R., Weininger, U., Meisl, G., Knowles, T. P. J., Leiding, T., Malmendal, A., Akke, M., and Linse, S. (2020) Ultrastructural evidence for self-replication of Alzheimer-associated Aβ42 amyloid along the sides of fibrils. *Proceedings of the National Academy of Sciences 117*, 11265–11273.

[79] Serpell, L. C. (2000) Alzheimer's amyloid fibrils: structure and assembly. *Biochimica et Biophysica Acta 1502*, 16–30.

[80] Xiao, Y., Ma, B., McElheny, D., Parthasarathy, S., Long, F., Hoshi, M., Nussinov, R., and Ishii, Y. (2015) Aβ(1–42) fibril structure illuminates self-recognition and replication of amyloid in Alzheimer's disease. *Nature Structural & Molecular Biology 22*, 499–505.

[81] Gremer, L., Schölzel, D., Schenk, C., Reinartz, E., Labahn, J., Ravelli, R. B. G., Tusche, M., Lopez-Iglesias, C., Hoyer, W., Heise, H., Willbold, D., and Schröder, G. F. (2017) Fibril structure of amyloid-β(1–42) by cryo–electron microscopy. *Science 358*, 116–119.

[82] Yang, Y. et al. (2021) Cryo-EM Structures of Amyloid-β 42 Filaments from Human Brain. *bioRxiv*

[83] Lutter, L., Aubrey, L. D., and Xue, W.-F. (2021) On the Structural Diversity and Individuality of Polymorphic Amyloid Protein Assemblies. *Journal of Molecular Biology 433*, 167124, From Protein Sequence to Structure at Warp Speed: How Alphafold Impacts Biology.

[84] Xue, W.-F., Homans, S. W., and Radford, S. E. (2009) Amyloid fibril length distribution quantified by atomic force microscopy single-particle image analysis. *Protein Engineering Design and Selection 22*, 489–496.

[85] Pogostin, B. H., Linse, S., and Olsson, U. (2019) Fibril Charge Affects α-Synuclein Hydrogel Rheological Properties. *Langmuir 35*, 16536–16544.

[86] Tycko, R. (2015) Amyloid Polymorphism: Structural Basis and Neurobiological Relevance. *Neuron 86*, 632–645.

[87] Frankel, R., Törnquist, M., Meisl, G., Hansson, O., Andreasson, U., Zetterberg, H., Blennow, K., Frohm, B., Cedervall, T., Knowles, T. P. J., Leiding, T., and Linse, S. (2019) Autocatalytic amplification of Alzheimer-associated Aβ42 peptide aggregation in human cerebrospinal fluid. *Communications Biology 2*, 365.

[88] Yates, E. V., Müller, T., Rajah, L., Genst, E. J. D., Arosio, P., Linse, S., Vendruscolo, M., Dobson, C. M., and Knowles, T. P. J. (2015) Latent analysis of unmodified biomolecules and their complexes in solution with attomole detection sensitivity. *Nature Chemistry 7*, 802–809.

[89] Jeffries, C. M., Ilavsky, J., Martel, A., Hinrichs, S., Meyer, A., Pedersen, J. S., Sokolova, A. V., and Svergun, D. I. (2021) Small-angle X-ray and neutron scattering. *Nature 1*.